RESEARCH ARTICLE

Developmental bias explains the evolutionary trend towards simple leaf shapes

James S Malone[1,2], Nora S Martin[3], Samuel HA von der Dunk[1], Liliana M Dávalos[4], Ard A Louis[1]*

[1]Rudolf Peierls Centre for Theoretical Physics, University of Oxford, Oxford, United Kingdom; [2]Department of Biology, University of Oxford, Oxford, United Kingdom; [3]CRG (Barcelona Collaboratorium for Modelling and Predictive Biology), Barcelona, Spain; [4]Department of Ecology and Evolution and Consortium for Inter-Disciplinary Environmental Research, Stony Brook University, Stony Brook, United States

eLife Assessment

This paper presents **important** findings on how the shapes of leaves might be biased towards simpler shapes due to biases in how variation is generated by developmental processes rather than selection. The authors present **convincing** evidence that combines image analysis of a herbarium dataset and computational analysis of a model of leaf development. The paper should be of interest to diverse researchers, ranging from plant development to the evolution of complexity more broadly.

***For correspondence:** ard.louis@physics.ox.ac.uk

Competing interest: The authors declare that no competing interests exist.

Funding: See page 16

Preprint posted
20 January 2026
Sent for Review
28 January 2026
Reviewed preprint v1
01 July 2026
Reviewed preprint v2
14 October 2026
Version of Record
24 November 2026

Reviewing Editor: Arvind Murugan, University of Chicago, United States

© Copyright Malone *et al*. This article is distributed under the terms of the Creative Commons Attribution License, which permits unrestricted use and redistribution provided that the original author and source are credited.

Abstract The relative influence of developmental bias and natural selection on evolutionary outcomes remains a central, unresolved question in evolutionary biology. Here, we combine large-scale phylogenetic trees with herbarium data to confirm that, across the evolutionary history of angiosperms, transitions from complex to simple leaf shapes have occurred at a significantly higher rate than the reverse. To investigate whether this directional trend reflects an underlying developmental bias, we simulate evolutionary transitions by introducing random mutations into a well-established computational model of leaf development. Despite excluding selection, the transition rates produced by the model closely align with those observed in the phylogenetic data. This agreement indicates that a strong developmental bias, reflecting the relative ease with which gene regulatory networks generate simple over complex leaves, has played a major role in shaping the evolution of leaf morphology. Our findings echo recent work showing that similar biases towards simplicity influence the evolution of molecular structures, including RNA secondary structures and protein quaternary assemblies. Together, these results suggest that a developmental bias favouring simplicity may be a widespread and general feature of evolutionary systems.

Introduction

Much of the phenotypic diversity across the tree of life can be explained by adaptation to ecological demands via natural selection. However, this process is constrained by the mechanisms that generate phenotypic variation, including development (***Smith et al., 1985***; ***Alberch, 1980***), which translates genetic information into form. While this idea is widely acknowledged in evolutionary developmental biology (***Smith et al., 1985***; ***Alberch, 1980***; ***Uller et al., 2018***), only recently have advances in methodology and our understanding of development allowed researchers to examine its predictive power

for evolutionary outcomes (**Alberch and Gale, 1985**; **Prusinkiewicz et al., 2007**; **Kavanagh et al., 2013**; **Hagolani et al., 2021**; **Johnston et al., 2022**; **Zimm et al., 2023**; **Staps et al., 2023**; **Rohner and Berger, 2023**). Yet it remains unclear how widespread and strong this developmental bias is across phylogeny (**Laland et al., 2014**; **Welch, 2017**), particularly for complex traits like morphology. Here, we test whether developmental bias can account for macroevolutionary patterns in angiosperm leaf shape evolution.

Angiosperm leaves are an attractive system to study developmental bias. They display vast morphological diversity, much of which can be effectively represented in only two spatial dimensions due to minimal growth along the adaxial-abaxial (upper-lower surface) axis (**Runions et al., 2017**). This diversity arises from variations in growth patterns regulated by gene regulatory networks (GRNs) that orchestrate both local and global growth dynamics during leaf development, allowing complex forms to emerge from anisotropic expansion. These processes include deeply conserved genes and developmental mechanisms (**Nikolov et al., 2019**). Variation in leaf morphology is driven not so much by changes in gene content, but rather by differences in the spatial and temporal expression of shared developmental regulators. This helps explain why closely related species can display wide variation in leaf shape. For instance, the genus *Pelargonium* includes species with unlobed, lobed, dissected, and compound leaves (**Nicotra et al., 2011**). Similarly, significant variation can occur within a single organism, as seen in *Morus alba* (mulberry), which produces both unlobed and lobed leaves, often with varying degrees of lobe symmetry (**Runions et al., 2017**; **Kidner and Umbreen, 2010**). The conservation of basic growth mechanisms also suggests that some developmental biases will be, to first order, shared across many different angiosperm species, enabling large-scale studies of the role of development in determining evolutionary outcomes.

At the same time, there is evidence that leaf shape can be influenced by ecological demands such as thermoregulation (**Vogel, 1970**; **Givnish, 1987**), hydraulic efficiency (**Sisó et al., 2001**), light interception (**Roden, 2003**; **Perez et al., 2018**; **Otto et al., 2025**), and herbivory (**Dell'Aglio et al., 2016**; **Higuchi and Kawakita, 2019**). However, it is still unclear how strong and general these effects are in natural environments (**Campitelli and Stinchcombe, 2013a**; **Leigh et al., 2017**). Size and the presence/absence of teeth on the margin are often stronger predictors of ecology than the broader leaf dissection categories we use here (**Sack and Frole, 2006**; **Scoffoni et al., 2011**; **Little et al., 2010**; **Peppe et al., 2011**; **Royer et al., 2012**; **Donoghue et al., 2022**; see *Appendix 5* for further discussion).

In a notable study, **Geeta et al., 2012** analysed a phylogeny of 561 predominantly angiosperm taxa, showing that most leaf shapes (76% in their sample—Table 2) are unlobed and that transition rates between leaf shapes are highly asymmetric. Specifically, transitions from more complex forms—such as lobed, dissected, or compound leaves—to simpler unlobed forms occurred far more frequently than transitions in the opposite direction. What explains this global bias towards simpler leaves? Is it primarily development or is it primarily adaptation?

In order to answer this question, we proceed with two parallel lines of work. In the first, we extend the phylogenetic analysis of **Geeta et al., 2012** with two much larger, recent phylogenies (**Janssens et al., 2020**; **Zuntini et al., 2024**) and our own shape classification dataset made from 8911 herbarium images (**Naturalis Biodiversity Center, 2024**). These confirm that transitions to unlobed leaves are much more likely than transitions away from unlobed leaves.

In the second line of work, we examine the role of random mutations using a well-established computational model of angiosperm leaf development by **Runions et al., 2017** (Figure 5). This model captures key conserved developmental mechanisms thought to be broadly shared across angiosperms (Methods: *Simulating leaf development*), allowing us to explore the generic effects of neutral evolution in the absence of direct selection on leaf shape. Remarkably, we find that random mutation alone is sufficient to reproduce the relative phylogenetic rates towards unlobed leaf forms. This suggests that developmental bias may be the first-order explanation of this macroevolutionary trend.

The basic mechanism driving this bias towards simplicity is straightforward (**Johnston et al., 2022**): complex leaf shapes need more tightly constrained GRNs than the simpler unlobed leaf shape (**Kierzkowski et al., 2019**). As a result, random genetic variation is more likely to produce simple shapes rather than complex ones that require more finely tuned parameter combinations.

Results

Transition rates from complex leaves to simple leaves are greater than the reverse across angiosperm phylogeny

To establish whether there is a phylogenetic bias towards simple, unlobed leaves, we inferred the rate of evolutionary transitions between different leaf shapes across angiosperm phylogeny. We first classified 8911 herbarium images (***Figure 1A***; ***Naturalis Biodiversity Center, 2024***) into four discrete categories—unlobed, lobed, dissected and compound. We used these data, as well as another shape classification dataset from ***Geeta et al., 2012***, to label the tips of five phylogenetic trees representing angiosperm evolution (***Geeta et al., 2012***; ***Janssens et al., 2020***; ***Zuntini et al., 2024***). Of these trees, three were resolved at the level of genus (***Zuntini et al., 2024*** genus, ***Janssens et al., 2020*** genus and ***Geeta et al., 2012***). The other two were resolved at the level of species (***Zuntini et al., 2024*** species and ***Janssens et al., 2020*** species) enabling us to examine how altering the amount of species-level diversity affects inferred transition rates. In agreement with ***Geeta et al., 2012***, we found that the vast majority of the taxa represented at the tips of these new phylogenies had unlobed leaves (Table 2), already suggesting a strong bias towards simple, unlobed leaves.

To infer the rates of evolution among these 4 categories while accounting for tree topology, we fitted a continuous-time Markov chain (CTMC) model to the labelled trees (Methods: *Inferring evolutionary rates from phylogeny*), using a Markov chain Monte Carlo (MCMC) approach implemented in BayesTraits V4.1.2 (***Pagel et al., 2004***). We detected significantly higher rates of transition to the simplest shape (unlobed) than away from it towards more complex shapes, as also found in ***Geeta et al., 2012***; ***Figure 1A*** and ***Appendix 1—figure 1A***.

The bias towards unlobed shapes was consistent across the five phylogenetic trees (***Appendix 1—figure 1A and B***). We found no cases where the direction of two statistically significant (black arrows—where 0 falls outside a 95% credible interval) net rates disagreed between phylogenies (***Appendix 1—figure 1A***).

A computational model of leaf development recapitulates in vivo experiments demonstrating developmental bias towards unlobed leaf shape

To investigate how much of the preference for unlobed leaves can be explained by developmental bias, we use a popular model from ***Runions et al., 2017*** that combines gene-regulatory networks and key growth mechanisms for leaf shape (Methods: *Simulating leaf development*). As a first validation test, we use the model to analyse in vivo experiments by ***Kierzkowski et al., 2019*** that identified a bias towards simpler leaf shapes in *Arabidopsis thaliana* and *Cardamine hirsuta*.

In particular, this study found that expression of the genes *SHOOTMERISTEMLESS* (*STM*) and *REDUCED COMPLEXITY* (*RCO*) together was necessary to generate the compound shape in *C. hirsuta* and sufficient to induce compound shape in *A. thaliana* (***Figure 2A***). Therefore, in this system, compound shape requires a more specific combination of gene expression than simpler shapes (e.g. lobed, unlobed).

While the ***Runions et al., 2017*** model was not designed to model this system specifically, we tested whether it could, nonetheless, reproduce the result from ***Kierzkowski et al., 2019*** by selecting two model parameters that control similar growth properties to the genes *STM* and *RCO*, total growth duration and morphogen repression strength, respectively (***Figure 2***). In agreement with the experiments, we found that activating both parameters together was sufficient to produce a compound shape while activating each in isolation was not (***Figure 2A and B***).

Having reproduced the experimental phenotypes, we next used the model to explore the *STM*/*RCO* parameter space in more detail, systematically varying morphogen repression strength and duration of growth within their biologically plausible ranges (***Figure 2C***). We found that the majority of this space (20 of 25 parameter combinations) was occupied by simple, unlobed shapes, with only a small fraction representing more complex shapes (1/25 dissected, 4/25 compound—see Methods: *Shape classification*). This agrees with ***Kierzkowski et al., 2019*** who also found that a similar fine-tuning is required for compound leaves.

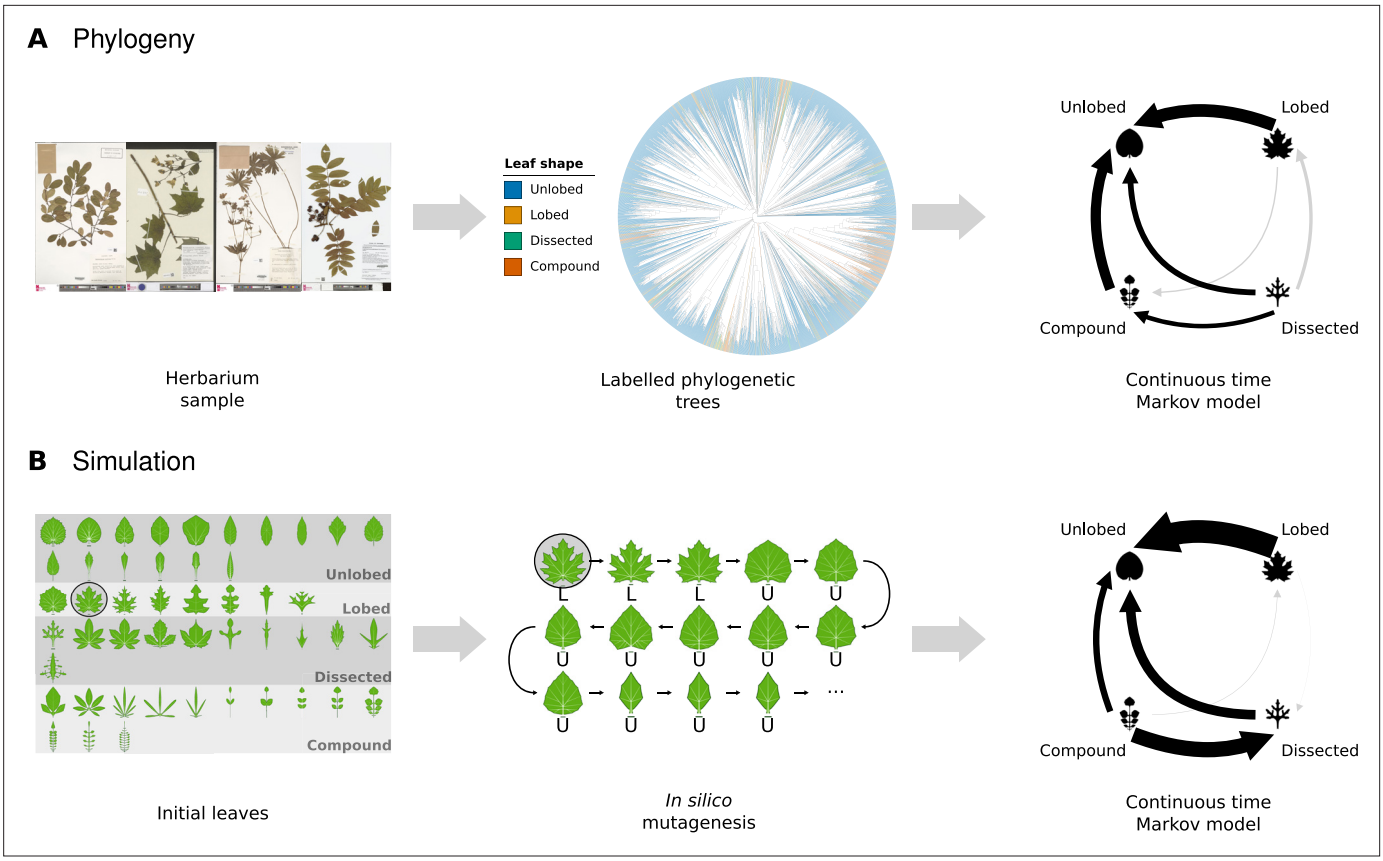

Figure 1. A summary of the methods and main results. We inferred transition rates between leaf shapes in two different ways: (**A**) by fitting a continuous-time Markov chain (CTMC) model of trait evolution to phylogenetic trees and (**B**) by simulating mutation in a computational model of leaf development. (**A**) (Left) Images sampled from the Naturalis Biodiversity Center herbarium (***Naturalis Biodiversity Center, 2024***; ***Plowman, 1981***; ***de Bruijn, 1981***; ***van Royen, 1973***; ***Bhikhi, 2011***) are manually classified as unlobed (u), lobed (l), dissected (d), or compound (c) (Methods: *Inferring evolutionary rates from phylogeny*). This dataset, as well as an analogous dataset by ***Geeta et al., 2012***, is used to label the tips of five different phylogenetic trees representing angiosperm evolution (***Geeta et al., 2012***; ***Janssens et al., 2020***; ***Zuntini et al., 2024***). (Centre) The ***Zuntini et al., 2024*** species tree is shown in full. Rates are inferred by fitting a CTMC model to the labelled trees using a Markov chain Monte Carlo (MCMC) approach in BayesTraits V4.1.2 (***Pagel et al., 2004***). (Right) Posterior net rates for the ***Zuntini et al., 2024*** species tree are shown as arrows. Black (grey) arrows depict rates for which 0 falls outside (within) a 95% credible interval. (**B**) (Left) An initial sample of 48 leaves representing a wide morphospace is generated using the ***Runions et al., 2017*** model (Methods: *Simulating leaf development and Generating the initial sample*). Leaves in this sample are mutated in parallel through a random walk algorithm, with no selection besides rejecting parameter combinations that give physically implausible leaves (***Table 1***), generating a sequence of leaves that evolve away from the initial leaf (Methods: *In silico mutagenesis*). (Middle) Every leaf is classified as unlobed (u), lobed (l), dissected (d), or compound (c) using an automated morphometric approach (Methods: *Shape classification*), giving a sequence of character states for each walk. To this trajectory, a CTMC model is fitted using MCMC (Methods: *Inferring evolutionary rates from random walk data*). (Right) Arrows depict posterior net rates for the MUT2 scheme (Algorithm 1).

The online version of this article includes the following figure supplement(s) for figure 1:

Figure supplement 1. ***Zuntini et al., 2024*** species tree.

Figure supplement 2. ***Zuntini et al., 2024*** genus tree.

Figure supplement 3. ***Janssens et al., 2020*** species tree.

Figure supplement 4. ***Janssens et al., 2020*** genus tree.

Figure supplement 5. ***Geeta et al., 2012*** tree.

Mutation in a computational model of leaf development is sufficient to reproduce phylogenetic bias towards simple leaves

The mechanism derived from the experiments on varying *STM/RCO*, shown in ***Figure 2***, is one specific driver of developmental bias. To investigate a wider range of possibilities, we study the effect of random mutations for a broad set of ***Runions et al., 2017*** model parameters (***Appendix 2—table***

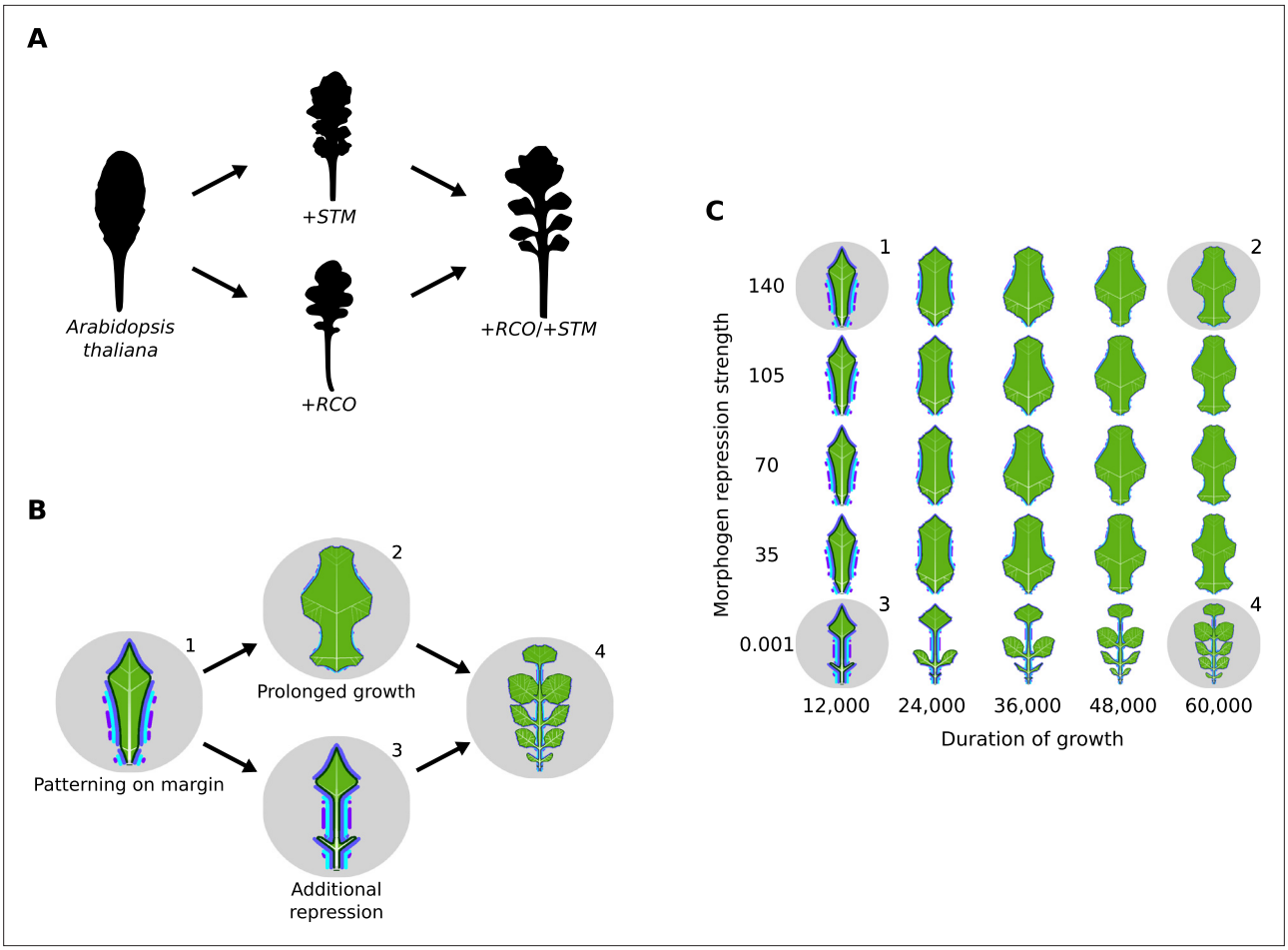

Figure 2. An experimentally motivated illustration showing that simple leaves are easier to generate than complex leaves. (**A**) Leaf silhouettes of wild-type *A. thaliana* and three mutants, which result in lobed (*+STM*, *+RCO*) and compound shape (+RCO/+STM) (reproduced from panel 3 of the graphical abstract of ***Kierzkowski et al., 2019***). Ectopic *STM* and *RCO* expression individually create a lobed shape, but together induce compound leaflets. (**B**) A reproduction of the ***Kierzkowski et al., 2019*** result using the ***Runions et al., 2017*** computational model of leaf development. *+STM* is approximated by increasing the duration of growth and *+RCO* by increasing the growth repression strength of one morphogen on the margin of the leaf. Morphogen presence is represented by the purple/blue lines outside the margin. (**C**) A morphospace showing the resulting shapes from different levels of the two parameters we use to approximate *STM* and *RCO*. The range shown for *morphogen repression strength* is the range in which biologically plausible shapes can be produced. Lower values correspond to stronger growth repression via decreased webbing. The range for *duration of growth* is the range in which leaves can be generated in a reasonable timeframe. In the parameter files of the ***Runions et al., 2017*** model, the parameters we refer to as *morphogen repression strength* and *duration of growth* are given by FAIRING4 and FINALFRAME, respectively.

1). We first generated a sample of initial leaves representing a diverse morphospace (***Figure 1B*** and ***Appendix 2—figure 6***). We mutated the initial sample using a random walk algorithm with two different mutational schemes, MUT2 (Algorithm 1) and MUT5 (Algorithm 2.2). These algorithms work by iterating through model parameters one by one and perturbing the value by a small amount. We then automatically classified the resulting shapes into the same four shape categories (unlobed, lobed, dissected, and compound) using a morphometric classifier (Figure 6). Of the 76,800 total leaves generated per simulation, we found that the proportions of unlobed, lobed, dissected and compound were 73.4, 9.6, 11.4, and 5.6%, respectively for MUT2 and 76.1, 7.2, 11.4, and 5.4% respectively for MUT5. This shows that our results are robust to the two different mutational schemes. Both reflect the fact that unlobed leaves occupy a significantly greater proportion of model parameter space that produces viable leaves than more complex shapes do (see also Results: *Complex leaves occupy a smaller volume in parameter space and are closer to simple leaves, but not vice versa*).

Regardless of the initial leaf shape, over the course of these random walks, the proportion of walks in an unlobed state increased to an equilibrium just below 80% while most other shape categories stabilise to a significantly lower proportion (***Figure 3*** and ***Appendix 1—figure 2***). These predictions

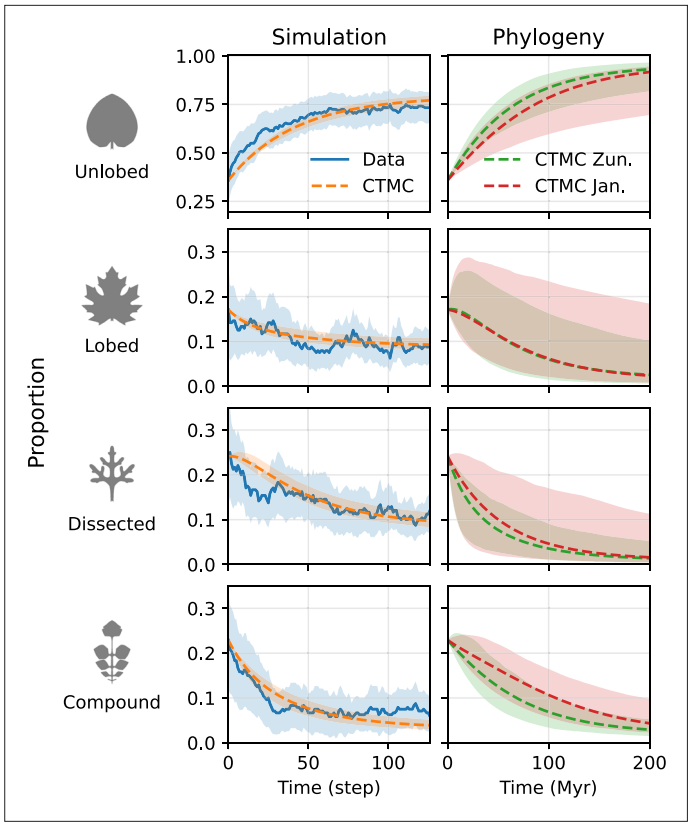

Figure 3. The proportions of each leaf shape over time as predicted by in silico mutagenesis and phylogeny. (*Simulation*) The solid blue line represents the mean proportion of random walk chains in each state at each time step ($\pm 1.96\times$ standard error) in our simulation (MUT2 Algorithm 1). To these data, we fitted a CTMC via maximum-likelihood estimation (MLE) (dashed line) and MCMC with errors inferred from MCMC posteriors via Monte Carlo error propagation. Since step size is arbitrary, for comparison with the phylogenetic model, we adjusted the x-limits for the simulation such that the CTMC predictions for both the simulation and phylogeny reach halfway from the initial distribution to the stationary distribution by approximately the same distance along the axis. (*Phylogeny*) We predict how the proportions of each leaf shape evolve from the same initial proportions used in the simulations, using the CTMC inferred from each phylogeny (green: ***Zuntini et al., 2024*** genus [***Figure 1—figure supplement 2***], red: ***Janssens et al., 2020*** genus [***Figure 1—figure supplement 4***]). Dashed lines represent the prediction using MLE transition rate values. Errors for all CTMC predictions were inferred from the transition rate MCMC posteriors using Monte Carlo error propagation ($N = 500$), and represent a 95% credible interval for each time step. We show these extrapolations for a time period equal to the approximate age of the angiosperm clade (200 Myr; ***Zuntini et al., 2024***).

The online version of this article includes the following figure supplement(s) for figure 3:

Figure supplement 1. MUT2 MCMC parameter trace.

Figure supplement 2. MUT5 MCMC parameter trace.

Figure supplement 3. ***Zuntini et al., 2024*** species MCMC parameter trace.

Figure supplement 4. ***Zuntini et al., 2024*** genus MCMC parameter trace.

Figure supplement 5. ***Janssens et al., 2020*** species MCMC parameter trace.

Figure supplement 6. ***Janssens et al., 2020*** genus MCMC parameter trace.

Figure supplement 7. ***Geeta et al., 2012*** MCMC parameter trace.

lie within the margins of error of the phylogeny-derived CTMC model predictions (***Figure 3*** and ***Appendix 1—figure 2***), suggesting that mutation and development alone are, to first order, sufficient to predict the relative frequency of different leaf shapes over evolutionary time.

To enable a more detailed comparison between simulation and phylogeny, we inferred the rates of shape transitions from our simulations. By estimating rates for all 12 possible (non-self) transitions, we gain deeper insight into the dynamics of shape change over time than by examining the

proportions of the four shape categories alone. To do this, we fitted the same CTMC model used for the phylogenetic inference to the random walk data, to estimate the evolutionary rates between shape categories in the absence of processes other than mutation, using MCMC (***Kalbfleisch and Lawless, 1985***; ***McGibbon and Pande, 2015***). In agreement with our phylogenetic inference, we found that transitions from unlobed occurred at a significantly lower rate than transitions to unlobed, giving a consistent net transition rate towards unlobed (***Figure 1B*** and ***Appendix 1—figure 1A***). This robust agreement between relative rates derived independently from simulations and phylogenies suggests that the evolutionary preference for simple leaves observed across angiosperm phylogeny may primarily be driven by developmental bias instead of selection.

By contrast, for transition rates between complex leaf shapes (lobed, dissected, and compound; ***Figure 1*** and ***Appendix 1—figure 1A***) there is less agreement both among the different phylogenies and between the phylogenies and the simulations. These differences could be because selection has played a more prominent role in the transitions among more complex leaf shapes than it has for transitions from complex to simple. The model may also be less reliable at resolving relative rates of

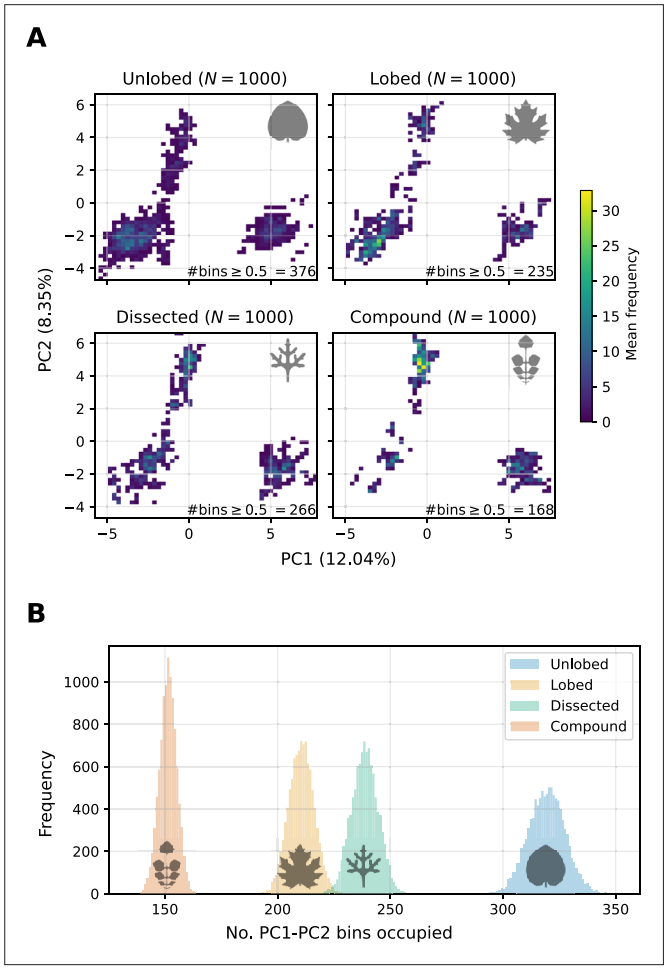

Figure 4. Simpler leaves occupy a greater volume than complex leaves in model parameter space. (**A**) A 2D histogram of model parameter space given by the two principal axes from a principal components analysis (PCA) of a sample of 4000 leaves from each shape category from one of the simulations (MUT2). Mean bin occupancy is calculated via a bootstrapping approach, by sub-sampling with replacement $N = 1000$ leaves from each shape category for 10,000 iterations. Bins are shaded if the mean occupancy across these iterations is ≥0.5. This illustrates how unlobed leaves occupy a larger region of model parameter space than more complex shapes and that this larger space also contains the majority of more complex leaves. Moreover, more complex leaves are concentrated within a much smaller area than unlobed leaves. (**B**) The number of PC1–PC2 2D histogram bins occupied by each leaf shape in 10,000 bootstrap samples ($N = 1000$) of a balanced sample of MUT2 (4000 per shape category). Bins with at least one leaf present are counted. This reveals that the unlobed category occupies by far the largest area in this 2D projection of parameter space. We find the same is true for other PCs (***Appendix 4—figure 1***).

complex leaves, for which more detail needs to be specified. Fully resolving the discrepancies for transitions between more complex leaf shapes would require reducing the error associated with the phylogenetic rate estimates, which in turn would necessitate significantly more leaf shape data.

Complex leaves occupy a smaller volume in parameter space and are closer to simple leaves, but not vice versa

To further investigate the mechanisms behind the bias towards simple leaves, we explored—much as we did for the experimentally inspired study in ***Figure 2C***—the relative volumes in parameter space that different shapes occupy. Projecting the parameter values of all random walk outputs into a 2D space via principal component analysis (PCA) reveals several possible factors affecting relative rates (***Figure 4***). First, it shows that the four shape categories occupy areas of different sizes (***Figure 4A***). The simplest category, unlobed, occupies by far the greatest area (***Figure 4B***), suggesting that the bias towards simple forms in our simulations can be partially explained because, as argued before (***Figure 2***), more parameter combinations map to simple leaves than complex leaves. We find that this pattern also holds for PC3–PC4 (***Appendix 4—figure 1E***) and PC5–PC6 (***Appendix 4—figure 1F***).

Moreover, the vast majority of lobed, dissected and compound leaves are contained within a broader area occupied by unlobed in the 2D parameter space (***Figure 4A***), suggesting that more complex leaves are close to simpler leaves in parameter space but not always vice versa. This provides another mechanism making transitions from complex leaves to simple leaves easier than the reverse. We also observe this same pattern for PC3–PC4 (***Appendix 4—figure 1B***) and PC5–PC6 (***Appendix 4—figure 1C***).

Finally, the parameter space of unlobed leaves appears to be much more connected than the space of more complex leaves. Constructing a nearest neighbour graph (no. neighbours = 6) from the PC1–PC2 parameter space reveals that unlobed separates into far fewer connected components (3) than lobed (131), dissected (96), and compound (235) (***Appendix 1—figure 3***). Repeating this analysis in the full-dimensional parameter space also yielded fewer connected components for unlobed than for the other categories. This may further contribute to the bias in transition rates towards unlobed, as less connected spaces would be more frequently exited by random walks than more connected spaces.

Our results show that the finding from experiments (***Kierzkowski et al., 2019***) and manual parameter searches (***Figure 2C***)—that simpler leaves occupy a larger volume within the parameter space of the developmental programme—extends to the ***Runions et al., 2017*** model more generally. This volume disparity, in addition to other properties including the degree of overlap between shape categories and the connectedness, may account for much of the bias towards unlobed we see in our simulations.

Discussion

We set out to test the hypothesis that mutation alone was sufficient to produce the higher transition rates towards simple leaves compared to complex leaves observed in angiosperm phylogeny (***Geeta et al., 2012***). By performing in silico mutagenesis, we found that non-adaptive processes alone produce greater transition rates to simple unlobed leaves than to complex leaf shapes such as lobed or compound (***Figures 1B and 3***). We also reproduced the observation from angiosperm phylogeny that unlobed leaves have evolved at a faster rate from complex leaves than vice versa (***Geeta et al., 2012***), using larger and more recent trees (***Janssens et al., 2020***; ***Zuntini et al., 2024***) and new classification data (***Figures 1A and 3***). Together, this suggests that a developmental bias towards simple, unlobed leaves can explain this macroevolutionary pattern in flowering plants.

Our finding is consistent with the growing body of evidence that developmental bias can play a significant role in evolutionary outcomes for morphological traits (***Alberch and Gale, 1985***; ***Prusinkiewicz et al., 2007***; ***Kavanagh et al., 2013***; ***Hagolani et al., 2021***; ***Johnston et al., 2022***; ***Zimm et al., 2023***; ***Staps et al., 2023***; ***Rohner and Berger, 2023***). The particular bias towards simplicity is consistent with recent work arguing for a generic bias towards descriptional simplicity in genotype-phenotype maps (***Johnston et al., 2022***). ***Johnston et al., 2022*** provided examples of this bias strongly affecting RNA secondary structure, where simpler structures are much more likely to be observed in nature than complex ones (see also ***von der Dunk et al., 2025***) and for self-assembling

protein quaternary structure, where this bias helps explain the prevalence of highly symmetric forms in the Protein Data Bank (PDB). Furthermore, this bias has been predicted to hold more widely for input-output maps (***Dingle et al., 2018***). This generic argument implies that the simplicity bias observed in molecular phenotypes may extend to the level of macroscopic phenotypes, which we show here for leaf shape, but also potentially to a much wider set of morphological phenotypes. More specifically, our results suggest that this bias towards simplicity may hold generically when development uses conserved mechanisms and GRNs where complex phenotypes need tighter parameter specification than simpler phenotypes.

Our study also opens up a number of future directions for studying the evolution of leaf shape. First, it would be valuable to repeat similar simulations in alternative models of leaf development (***Bilsborough et al., 2011***; ***Kierzkowski et al., 2019***; ***Kuchen et al., 2012***). The ***Runions et al., 2017*** model is uniquely suited to macroevolutionary studies such as this one, as it captures key conserved elements of angiosperm leaf development while generating a large morphospace, but if the same bias towards simplicity were observed in other models, this would provide further evidence that it is a general property of leaf development. Second, it would be illuminating to conduct similar in silico mutagenesis, but classify the resulting leaves using a continuous classification system instead of discrete categories, such as directly measuring margin complexity using a compression algorithm on the leaf silhouette (***Martin et al., 2024***). This could help identify more subtle biases between different leaf forms, including teeth/serrations, which we do not analyse here, but which the model can produce (***Figure 1B*** and ***Appendix 2—figure 6***). Third, when inferring transition rates from phylogeny, we were limited by the availability of herbarium data, the resolution of phylogenetic trees and the rate at which herbarium leaves could be manually classified. To more accurately resolve transition rates between more complex shape categories, it would be useful to repeat this study with larger phylogenies. This would likely require an automated method for herbarium shape classification. Finally, the methodology presented in this study—combining phylogenetic analysis with evolutionary and developmental computational models—could be used to study the evolution of other traits where a reliable developmental model exists, and phylogenetic data are available (e.g. ***Prusinkiewicz et al., 2007***). This

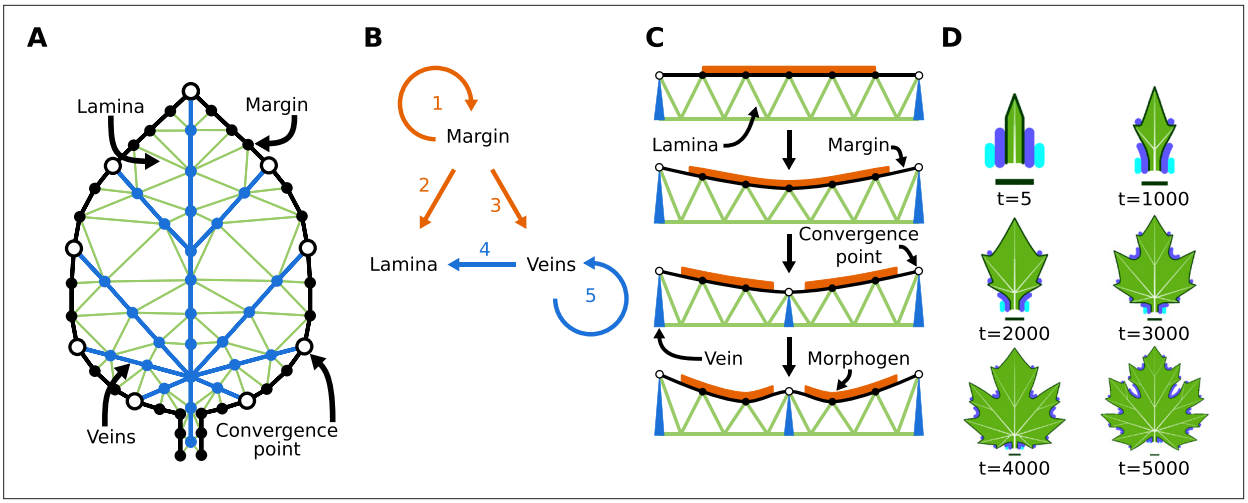

Figure 5. A description of the leaf model from ***Runions et al., 2017***, highlighting the three key components of leaf development and their interactions. (**A**) Model components illustrated in leaf form (inspired by ***Runions et al., 2017***, ***Figure 3***). Margin in black, veins in blue, lamina in green, convergence points in white with black outlines. (**B**) The three components of the model with arrows indicating interactions that affect growth. (1) Existing morphogens and convergence points influence where new ones will form. (2) Convergence points and morphogens influence local growth rate. (3) Convergence points induce new veins. (4) Veins determine local growth direction. (5) Existing veins influence the growth of new veins. (**C**) Zoomed view of the margin, showing how growth of the vasculature and patterning on the margin interact to produce protrusions and sinuses. Veins (in blue) extend, pushing the margin out; however, a morphogen (in orange) inhibits webbing between the veins, causing a sinus to form. This increases the distance between the two convergence points, leading to the insertion of another convergence point between the two that excludes the morphogen from its vicinity. Existing vasculature connects to the convergence point and specifies a new axis of growth. (**D**) Different growth stages of a model leaf. The dark blue morphogen inhibits webbing and convergence point formation; the light blue morphogen delineates the petiole. The value of *t* denotes the iteration of the simulation.

would greatly expand our understanding of how well development can predict trait evolution across phylogeny.

Methods

Simulating leaf development

We use a well-established model by ***Runions et al., 2017*** to approximate the developmental programme underpinning angiosperm leaf shapes. In this model, leaves are represented in 2D as three components (***Figure 5A and B***). First, an open tree structure with growing edges to which new edges are added, representing the vasculature; second, a polygon with morphogen presence or absence at each vertex that deforms according to the growing vasculature and instructs the initiation of new veins, representing the margin; third, a passive triangular mesh representing the lamina that fills the space inside the margin.

Many similar models capture a narrow range of shape diversity—for example, variation within *A. thaliana* (***Kuchen et al., 2012***; ***Bilsborough et al., 2011***). On the other hand, the ***Runions et al., 2017*** model captures a broad spectrum of leaf shapes within a single parameter space. This enables the inference of transition rates between highly divergent shapes such as unlobed and compound. However, it also introduces challenges as the genetic basis of leaf shape differs among lineages and remains poorly resolved for many non-model species. To address this, the ***Runions et al., 2017*** model is formulated at the level of developmental mechanism rather than specific genes. It is therefore important to understand that this model is limited in what it can tell us about leaf development and evolution at the level of specific genes.

Growth in the ***Runions et al., 2017*** framework is a product of two key developmental mechanisms. The first is morphogen patterning on the leaf margin. The margin—the tissue at the adaxial-abaxial boundary—has long been recognised as a critical site for patterning during leaf development. For example, auxin patterns marginal outgrowths in *Solanum* (***Koenig et al., 2009***), *A. thaliana* (***Bilsborough et al., 2011***) and *C. hirsuta* (***Barkoulas et al., 2008***). The products of genes such as *CUC2* in *A. thaliana* (***Bilsborough et al., 2011***) or *RCO* in *C. hirsuta* (***Kierzkowski et al., 2019***) also localise to the margin and determine whether these auxin-driven outgrowths form serrations, lobes or leaflets. The closely related *CUC3* and *NO APICAL MERISTEM* (*NAM*) genes localise to leaflet primordia boundaries, and their down-regulation reduces serration and lobing in diverse lineages, namely *Aquilegia caerulea*, *Pisum sativum*, *C. hirsuta*, *Solanum lycopersicum,* and *Solanum tuberosum* (***Blein et al., 2008***). Although the role of auxin in patterning protrusions is highly conserved, many other developmental regulators are not conserved across phylogeny. For example, *RCO* is only present in the Brassicaceae family (***Vlad et al., 2014***) and therefore plays no role in determining leaf shape in other compound lineages such as *Solanum*. Furthermore, there are likely many other genes regulating leaf shape in non-model species that are currently unknown. The model accounts for this variation and uncertainty by not assuming a conserved identity for the morphogens. Both the number of morphogens present and their effect on growth can vary according to their associated parameter values. What is assumed to be conserved is the broader principle that growth-modifying morphogens form patterns along the margin.

The second key mechanism that the model incorporates is the alignment of local growth direction with veins. This is consistent with the telome theory (***Zimmermann, 1952***), according to which leaves first evolved by the webbing of tissue between shoots, as well as a number of lines of empirical evidence. At the tissue level, deeply dissected leaves (e.g. *Pelargonium carnosum*) necessarily align growth directions with main veins and variegated leaves also show growth orientations that track major veins (***Runions et al., 2017***). At the molecular level, auxin has been shown to pattern veins (***Scarpella et al., 2010***; ***Scarpella, 2024***) as well as marginal outgrowths (***Bilsborough et al., 2011***; ***Barkoulas et al., 2008***; ***Koenig et al., 2009***) in model species, consistent with the model assumption that vein growth drives margin growth. In the ***Runions et al., 2017*** model, consistent with observed patterns of auxin efflux carriers in *A. thaliana* (***Scarpella et al., 2006***), new veins are inserted between the current vasculature and special points on the margin known as 'convergence points'. New convergence points form between old convergence points depending on the distance between old points and the effect of any morphogens present (***Figure 5C***). This is an extension of Hofmeister's rule (***Kirchoff, 2003***) for leaf primordium emergence in the shoot apical meristem, where new primordia

Table 1. Random walk constraints.

The only type of selection we apply during the walk is stabilising selection for physically plausible leaves. See ***Appendix 2—figure 8*** for examples of rejected leaves. *Weight difference* (***Appendix 2—figure 8A***) ensures that the midvein and petiole are roughly in line with the centre of mass of the leaf. *Leaf width* (***Appendix 2—figure 8B***) ensures that leaves which stop growing after the first few stages of the model simulation are rejected. *Veins outside lamina* (***Appendix 2—figure 8C***) prevents leaves forming whose veins grow outside the lamina. *Veins width* (***Appendix 2—figure 8D***) and *veins area* (***Appendix 2—figure 8E***) ensure that leaves that generate without adequate vasculature are rejected. *Overlapping margin* (***Appendix 2—figure 8F***) rejects leaves with ingrown margins. *Error or timeout* – some parameter combinations result in the simulation exiting unexpectedly or taking a very long time to complete, posing an additional constraint.

Check	Condition
Weight difference	The difference in leaf area either side of the midvein must not exceed 6% of the total leaf area.
Leaf width	Final leaf must be wider than 110% of the width of the leaf at the first iteration of the growth simulation.
Veins outside lamina	Less than 3.7% of the total vein area can be non-overlapping with the lamina.
Veins width	The maximum width of the vasculature must be greater than 5% of the total image width.
Veins area	The proportion of total leaf area that is occupied by veins must be greater than 5%.
Overlapping margin	The proportion of the lamina (interior area of the leaf) that is occupied by leaf margin must be less than 0.1%.
Error or timeout	Simulation exits unexpectedly or lasts longer than 160 s.

emerge in the largest space between existing primordia. Some properties of veins are not captured by the model, specifically closed reticulate and parallel vein architectures. This is partly because there is some uncertainty surrounding the mechanisms by which these architectures form (***Scarpella, 2024***; ***Perico et al., 2022***), but we acknowledge this as a limitation of the model.

More broadly, much of our understanding of leaf development derives from a small number of model species. These have revealed some conserved genes and mechanisms (***Bar and Ori, 2014***), but many details are lineage-specific (***Vlad et al., 2014***). Consequently, some unavoidable uncertainty remains in how well the ***Runions et al., 2017*** model captures global trends.

Generating the initial sample

Since a range of different forms are contained within each shape category, we began our simulations from leaves drawn from an initial sample representing a wide variety of morphologies (16 unlobed, 8 lobed, 11 dissected, 13 compound; ***Figure 1B*** and ***Appendix 2—figure 6***). This sample was generated using a variety of methods. Some leaves were taken from ***Runions et al., 2017***; others were generated by tuning parameters by hand and some were taken from the output of random walks on leaves from ***Runions et al., 2017***.

In silico mutagenesis

To simulate mutation in our sample, we used a constrained random walk algorithm. The algorithm samples the parameter space of biologically plausible leaf shapes surrounding the starting leaf by making a small change to one of the parameters, checking the validity of the resultant leaf (***Table 1***), and then moving on to another parameter (see ***Appendix 2—figure 8*** for examples of rejected leaves). We chose this approach over other methods, such as uniform sampling or Latin hypercube sampling, as the biologically relevant ranges of each parameter were unknown. Random walks have been shown to cause some biases towards high-robustness regions of parameter space in discrete parameter spaces represented as networks (***van Nimwegen et al., 1999***), which in this case would result in the under-representation of invalid leaves. We have no reason to assume that this would

systematically bias the rates between valid leaves, but this cannot be fully excluded. For each of the 48 leaves in our initial sample (***Appendix 2—figure 6***), we ran 5 random walks for 320 steps, generating a total of $5 \times 48 \times 320 = 76{,}800$ leaves per simulation. We allow 100/122 model parameters to vary throughout the simulations (***Appendix 2—table 1***). Not all parameters are included, as some are not relevant to leaf shape (e.g. they control how the image is rendered).

To test the robustness of our results, we repeated the simulation with 2 different mutational schemes. MUT2 (Algorithm 1) iterates through the parameters in a random order, and attempts to change the parameter by a value selected at random from an array of numbers randomly generated at three different orders of magnitude. MUT5 (Algorithm 2.2) is the same as MUT2 except that each mutation is additionally scaled by 10% of the current parameter's range within the initial leaves (***Appendix 2—figure 6***). The aim here was to provide some way of accounting for the biologically relevant sampling range.

Algorithm 1: Random walk MUT2

```
θ ← initial parameter values
for step ← 0 to N_maxGenerated − 1 do
    for attempt ← 0 to N_maxAttempts − 1 do
        θ′ ← θ                                          // Copy parameters for this step
        mutation ← random draw from {
          uniform[0.1, 1),
          uniform[1, 10),
          uniform[10, 100)
        }
        sign ← random choice from {−1, 1}
        i ← random draw from {0,…,length(θ)−1}
        θ′[i] ← θ[i] + (mutation × sign)                // Mutate
        Run simulation with θ′
        if leaf passes sanity checks then
            θ ←θ′                                       // Save new parameters
            break
```

Shape classification

To sort the leaves into each of the four shape categories (unlobed, lobed, dissected, and compound), we developed a computer-vision program (***Figure 6***) to reduce error from subjectivity. It finds the coordinates of key landmarks in the leaf image, extracts morphometric measurements and assigns a category based on threshold values of these measurements (***Equation 1***). These morphometric measurements were also used to check if leaves were valid (***Table 1***) in the random walk algorithm.

First, the main visual features are extracted from the leaf image, including silhouette, margin, lamina and veins. The coordinates of each pixel along the edge of the silhouette (the contour) are extracted. A reference point is defined in the centre of the mid-vein at the point where it first branches outwards into lateral veins (***Figure 6B***). Then, the distance between each point on the contour and this reference point is calculated (***Figure 6C***). The local maxima and minima in this distance array that pass a certain prominence threshold are determined using `find_peaks` from the scipy.signal package with `distance=10` and `prominence=25`. These pertinent extrema represent estimates for the coordinates of the tips and sinuses of any protrusions in the leaf margin (***Figure 6B*** shown in orange and blue). Because of the prominence threshold, small protrusions such as serrations are excluded.

From the coordinates of the local minima, maxima and the reference point, we calculate a number of morphometric measurements which are then used to classify the leaf. Three measurements are used: ϵ, the total number of pertinent local maxima and minima; α, the average angle formed by each local maximum and its two adjacent minima; and ω, the average horizontal distance between each pair of local minima, closest to the midvein, that share the same vertical coordinate (measured in pixels). The definitions for each of the shape categories are as follows:

$$\left.\begin{array}{l}(\epsilon > 5 \wedge \alpha < 8^{\circ}) \vee \\ (\epsilon > 5 \wedge \omega < 25 \text{ pixels})\end{array}\right\} \implies \text{Compound (c)},$$
$$\epsilon > 5 \wedge \alpha < 30^{\circ} \implies \text{Dissected (d)},$$
$$\epsilon > 5 \wedge \alpha < 60^{\circ} \implies \text{Lobed (l)},$$
$$\epsilon \leq 5 \vee \alpha > 60^{\circ} \implies \text{Unlobed (u)}. \quad (1)$$

Any leaf that fails to satisfy any of these conditions is labelled as 'unclassified'. However, there were no unclassified leaves in either the MUT2 or MUT5 simulation.

Leaf shape is a continuous trait. Thus, the boundaries between discrete categories, such as those in ***Equation 1***, are arbitrary. This makes it difficult to assess the accuracy of the classifier algorithm. Nevertheless, we wanted to have some measure of how closely it matches classification by eye. Therefore, we manually classified 200 leaves randomly selected from one of the simulations, with an approximately equal number from the output of each initial leaf. 78.5% of the manually ascribed labels matched those assigned by the classifier (see ***Appendix 2—figure 7*** for further details). For comparison, we fitted a machine learning algorithm (Histogram-based Gradient Boosting Classification Tree from the scikit-learn Python package) to a sample of 500 manually labelled leaves, sampled in the same way as the set of 200. The algorithm was trained on the distance of 200 equally spaced points along the leaf contour to the reference point for each leaf (***Figure 6C***). When used to predict shape for the same sample of 200 leaves used for the threshold classifier, it returned an accuracy of 73.0%. We then repeated the machine learning approach using morphometric data rather than contour data, which returned an accuracy of 79.5%. This suggests that the threshold classifier is a good enough match with subjective shape classification compared to other classification methods. It also demonstrates that the morphometrics used to construct the original classifier are useful features when classifying shape as

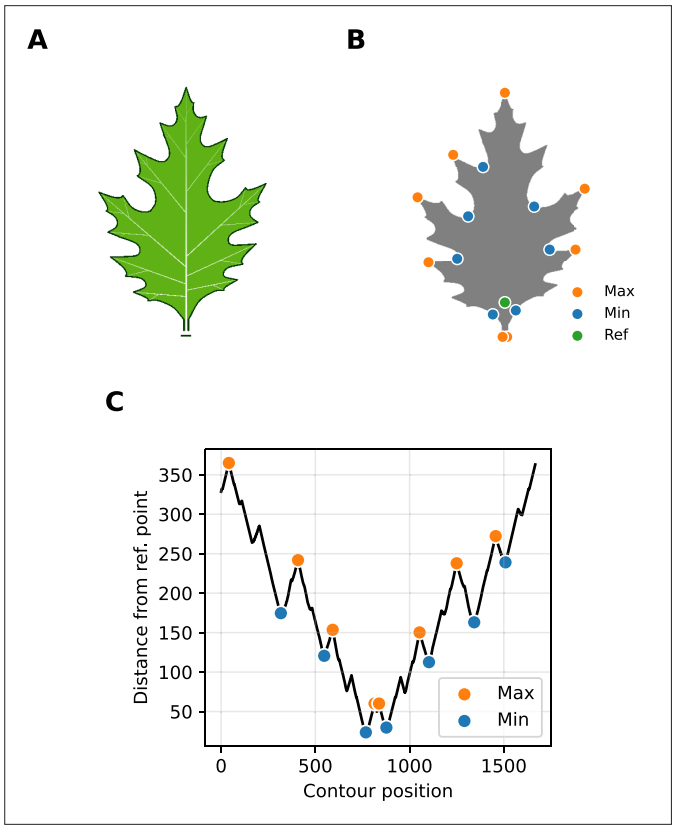

Figure 6. A summary of the morphometric classifier. (**A**) Example lobed leaf. (**B**) Silhouette with local maxima in orange, minima in blue, and reference point in green. (**C**) Graph of distances of each contour point to the reference point. Local maxima shown in orange, minima in blue.

unlobed, lobed, dissected or compound. The two machine-learning methods agreed on 77.0% of the labels.

Inferring evolutionary rates from random walk data

To test the model for bias in leaf shape transition rates upon mutation, we ran 5 random walks on each of the 48 initial leaves, for 320 steps, generating a total of 76,800 leaves for each of MUT2 and MUT5. Using the classifier (***Figure 6***), we assigned each leaf the category unlobed, lobed, dissected or compound (***Equation 1***). Evolutionary rates between shape categories were inferred by fitting a CTMC to the labelled walks.

This model is defined by a matrix of transition rates $\boldsymbol{Q}$ between each state—unlobed (u), lobed (l), dissected (d), and compound (c),

$$\boldsymbol{Q} = \begin{bmatrix} \sum_{\theta\in\{l,d,c\}} -q_{u\theta} & q_{ul} & q_{ud} & q_{uc} \\ q_{lu} & \sum_{\theta\in\{u,d,c\}} -q_{l\theta} & q_{ld} & q_{lc} \\ q_{du} & q_{dl} & \sum_{\theta\in\{u,l,c\}} -q_{d\theta} & q_{dc} \\ q_{cu} & q_{cl} & q_{cd} & \sum_{\theta\in\{u,l,d\}} -q_{c\theta} \end{bmatrix} \tag{2}$$

where the diagonal elements must be equal to the negative sum of all other elements in the same row (***Pagel, 1994***).

The model assumes that at any given instant, over a continuous-time interval, the system is in one of these four states. The probability $p(i,j,t)$ of transitioning between state i and j depends only on the current state, the transition rate matrix $\boldsymbol{Q}$ and the time t until the end of the transition. The matrix of all possible transition probabilities $\boldsymbol{P}(t)$ relates to $\boldsymbol{Q}$ and t as follows (***Kalbfleisch and Lawless, 1985***; ***Pagel, 1994***)

$$\boldsymbol{P}(t) = \exp(\boldsymbol{Q}t). \tag{3}$$

Therefore, the probability of a transition from state i to j over time t is

$$p(i,j,t) = \exp(\boldsymbol{Q}t)_{ij}. \tag{4}$$

The probability of a set of observed walks $x = \{x_0, x_1, ..., x_W\}$, where each walk contains a sequence of labelled steps $x_w = \{x_{w0}, x_{w1}, ..., x_{wN}\}$, given a particular set of rate parameters $\boldsymbol{Q}$ is

$$P(x|\boldsymbol{Q}) = \prod_{w=0}^{W} \prod_{n=0}^{N-1} p(x_{wn}, x_{w(n+1)}, t), \tag{5}$$

where w and n are walk and step indices, respectively. We assume $t = 1$ for every step, as over the course of the entire random walk, the average step size in parameter space will be approximately constant.

Rates were inferred from the random walk simulation data by sampling the posterior distribution of $\boldsymbol{Q}$ using MCMC, implemented with the emcee package for Python (***Foreman-Mackey et al., 2013***). We ran 24 chains for 5000 steps with uniform priors between 0 and 0.1 for all transition rates. The first 2500 steps from each chain were discarded and the remaining part thinned by removing all but every 10th step to obtain the posterior distribution (***Figure 3—figure supplements 1 and 2***). We took the mean of the posterior for each transition as the estimate for each transition rate in ***Figure 1***. As an additional check, we also inferred the rates via maximum-likelihood estimation (MLE) and found that they converged with the MCMC estimates (***Appendix 1—figure 1A and B***).

Because the inferred rates depend on the unit of time, we needed to normalise the transition rates to compare with the rates inferred from phylogeny. We did this for each mutational scheme by dividing by the mean of all transition rate estimates q_{ij}. We define a normalised rate as

$$\hat{q}_{ij} = \frac{q_{ij}}{\bar{q}},$$
$$\bar{q} = \frac{1}{12} \sum_{\substack{i,j\in\{u,l,d,c\} \\ i\neq j}} q_{ij}. \tag{6}$$

Inferring evolutionary rates from phylogeny

Although ***Geeta et al., 2012*** had already inferred rates between these 4 categories with a phylogeny of 561 taxa, we wanted to test how robust these results are. Those results used a phylogeny that is now more than 25 years old (***Soltis, 2000***), and there are now much larger (e.g. ***Zuntini et al., 2024***—9506 species) and more reliable phylogenies available. To do this analysis, we combined two phylogenetic trees (***Janssens et al., 2020***; ***Zuntini et al., 2024***) with leaf images from the Naturalis herbarium (***Naturalis Biodiversity Center, 2024***). We first filtered all digitised records to just those from angiosperm families as per APG IV (***The Angiosperm Phylogeny Group, 2016***). We then removed all but the first record for each species.

To see how the rates are affected by looking at the species-level versus the genus-level, we generated two trees for each original tree, one with species at the tips and one with all but one tip per genus removed. For the species-level trees, we took the intersection between the filtered herbarium data and the full trees. If more than 3100 tips remained, we sampled at random 3100 tips, to allow for manual classification within reasonable time limits. This gave a combined set of 5552 leaf images to classify for both species trees. Notably, the intersection between the herbarium data and the ***Zuntini et al., 2024*** species tree gave 3057 taxa. Since this was less than 3100, no further sub-sampling was required, and so unlike all the other trees in this analysis, the ***Zuntini et al., 2024*** species tree represents the raw intersection between the original tree and the herbarium. For this phylogeny, our genus tree and our species tree should both have similar levels of reliability. For the ***Janssens et al., 2020*** phylogeny, we trust the genus-level tree more than the species-level tree, because the overlap with the herbarium data was not as good at the species-level. For example, taxa were more heavily concentrated in a smaller number of angiosperm families, compared to the other trees (***Appendix 3—figure 1***). Moreover, we sub-sampled down to 3100 taxa from 16,436 in the raw intersection to make manual classification feasible—something not required for the other trees.

For the genus-level trees, we further sub-sampled the angiosperm filtered herbarium data to 200 records per family, or the maximum if fewer than 200 records were present. The purpose of this step was to sample more evenly over phylogeny, accounting for potential biases in the herbarium. We then took the intersection between genera in this sample and each of our phylogenies and randomly selected one species from within each genus that was present in the herbarium to use as the label. This gave a combined set of 3359 leaf images to classify across both genus trees.

These images were then used to classify each species as one of the four categories (unlobed, lobed, dissected, or compound) or ambiguous. This was done by eye, relying on a sample of model leaves and their morphometric classifier output for reference (***Figure 1B*** and ***Appendix 2—figure 6***). After classification, all species labelled as ambiguous were removed, leaving an unambiguously labelled phylogeny (***Table 2*** and ***Figure 1—figure supplements 1–5***).

We used 3 different phylogenies from the literature to infer the evolutionary rates. First, to compare our predictions directly to the ***Geeta et al., 2012*** study, we used the same phylogeny as in their analysis (***Soltis, 2000***), which is based on 3 genes: nuclear 18S rDNA and the plastid genes *rbcL* and *atpB*. Second, we used a tree by ***Janssens et al., 2020***, inferred using the plastid genes *rbcL* and *matK* (including *trnK*) and calibrated with 56 fossils. This tree comprises 36,101 species, representing 8399 genera, 426 families and all orders of flowering plants (available in Supplementary material 5 of ***Janssens et al., 2020***). Finally, we used a recent phylogeny by ***Zuntini et al., 2024***, containing 9506 species (7923 genera and all angiosperm families and orders), inferred using 353 nuclear genes and calibrated with 200 fossil records (available at https://zenodo.org/records/10778207; we used the

Table 2. The number of taxa in each shape category for each labelled tree used in our inference.
Columns with multiple shape categories (e.g. ld) represent taxa which could fit into any of the listed categories.

Tree	Unlobed (u)	Lobed (l)	Dissected (d)	Compound (c)	ld	lc	ldc	No. tips
Geeta et al., 2012	428 (76.3%)	38 (6.8%)	17 (3.0%)	68 (12.1%)	7 (1.2%)	1 (0.2%)	2 (0.4%)	561
Zuntini et al., 2024 species	2445 (86.0%)	102 (3.6%)	83 (2.9%)	212 (7.5%)	-	-	-	2842
Zuntini et al., 2024 genus	1910 (88.3%)	82 (3.8%)	47 (2.2%)	123 (5.7%)	-	-	-	2162
Janssens et al., 2020 species	2606 (87.2%)	125 (4.2%)	99 (3.3%)	160 (5.4%)	-	-	-	2990
Janssens et al., 2020 genus	2178 (88.6%)	97 (3.9%)	55 (2.2%)	128 (5.2%)	-	-	-	2458

tree 4-young-tree-smoothing-10-pruned-for-diversification-analyses). We show results from the ***Geeta et al., 2012*** phylogeny, labelled with their own classification data and the ***Janssens et al., 2020*** and ***Zuntini et al., 2024*** trees labelled with our own classification data from ***Naturalis Biodiversity Center, 2024***.

Rates were inferred using the MultiState method from BayesTraits V4.1.2 (***Pagel et al., 2004***). We used MCMC for 1,100,000 iterations with a sample period of 1000 and removed the first 100,000 iterations to obtain posterior distributions. We used a uniform prior between 0 and 0.1 for the ***Zuntini et al., 2024*** trees (***Figure 3—figure supplements 3 and 4***) and ***Janssens et al., 2020*** trees (***Figure 3—figure supplements 5 and 6***). However, for the ***Geeta et al., 2012*** tree, because branch lengths are measured in substitutions per site rather than millions of years, we instead used a uniform prior between 0 and 100 (***Figure 3—figure supplement 7***). We took the mean of each posterior as the transition rate estimate. In addition, we estimated the rates using MLE for comparison (***Appendix 1—figure 1A and B***). As the units of time differ between our phylogenies and the simulations, we needed to normalise the rates to allow for comparison. We did this using the same method as for the simulations (***Equation 6***): by dividing each transition rate estimate by the mean transition rate estimate for each tree.

Acknowledgements

JSM was supported by funding from the Biotechnology and Biological Sciences Research Council (UKRI-BBSRC) [grant number BB/T008784/1]. LMD was supported, in part, by National Science Foundation OISE 2020577 and a Stony Brook University Presidential Innovation and Excellence Fund. SvdD and NSM were supported by the Issachar Fund. NSM acknowledges support of the Spanish Ministry of Science and Innovation through the Centro de Excelencia Severo Ochoa (CEX2020-001049-S, MCIN/AEI/10.13039/501100011033), the EMBL partnership and the Generalitat de Catalunya through the CERCA programme. Research for this publication has been partially carried out in the Barcelona Collaboratorium for Modelling and Predictive Biology. This research is part of grant JDC2022-049526-I to NSM, funded by MCIU/AEI/10.13039/501100011033 and by 'European Union NextGenerationEU/PRTR'.

Additional information

Funding

Funder	Grant reference number	Author
Biotechnology and Biological Sciences Research Council	BB/T008784/1	James S Malone
Office of International Science and Engineering	2020577	Liliana M Dávalos
Stony Brook University	Presidential Innovation and Excellence Fund	Liliana M Dávalos
Issachar Fund		Nora S Martin Samuel HA von der Dunk
European Molecular Biology Laboratory		Nora S Martin
Generalitat de Catalunya		Nora S Martin
Centro de Excelencia Severo Ochoa	CEX2020-001049-S	Nora S Martin
Ministerio de Ciencia, Innovación y Universidades	JDC2022-049526-I	Nora S Martin

The funders had no role in study design, data collection and interpretation, or the decision to submit the work for publication.

Author contributions

James S Malone, Conceptualization, Software, Validation, Investigation, Visualization, Methodology, Writing – original draft, Project administration, Writing – review and editing; Nora S Martin, Conceptualization, Supervision, Investigation, Methodology, Writing – review and editing; Samuel HA von der Dunk, Investigation, Methodology, Writing – review and editing; Liliana M Dávalos, Resources, Methodology, Writing – review and editing; Ard A Louis, Conceptualization, Supervision, Project administration, Writing – review and editing

Author ORCIDs

James S Malone https://orcid.org/0009-0002-6243-3218
Nora S Martin https://orcid.org/0000-0003-4026-0985
Samuel HA von der Dunk https://orcid.org/0000-0002-5741-7558
Liliana M Dávalos https://orcid.org/0000-0002-4327-7697
Ard A Louis https://orcid.org/0000-0002-8438-910X

Peer review material

Version of Record:
Reviewer #1 (Public review): https://doi.org/10.7554/eLife.110692.3.sa1
Author response https://doi.org/10.7554/eLife.110692.3.sa2

Reviewed preprint v2
Reviewer #1 (Public review): https://doi.org/10.7554/eLife.110692.2.sa1
Author response: https://doi.org/10.7554/eLife.110692.2.sa0
eLife Assessment https://doi.org/10.7554/eLife.110692.2.sa2

Reviewed preprint v1
Reviewer #1 (Public review): https://doi.org/10.7554/eLife.110692.1.sa2
Reviewer #2 (Public review): https://doi.org/10.7554/eLife.110692.1.sa1
Author response: https://doi.org/10.7554/eLife.110692.1.sa0
eLife Assessment https://doi.org/10.7554/eLife.110692.1.sa3

Additional files

Supplementary files

MDAR checklist

Data availability

The code, numerical simulation results and leaf-shape classifications used in the analyses presented in this paper are openly accessible at https://github.com/malonej501/leaf-shape-evolution, copy archived at ***Malone, 2026***. Sources and access details for the reused Naturalis herbarium records and published phylogenetic datasets are provided in Methods, "Inferring evolutionary rates from phylogeny".
The following previously published datasets were used: ***Zuntini and Carruthers, 2024***

References

Alberch P. 1980. Ontogenesis and morphological diversification. *American Zoologist* **20**:653–667. DOI: https://doi.org/10.1093/icb/20.4.653

Alberch P, Gale EA. 1985. A developmental analysis of an evolutionary trend: digital reduction in amphibians. *Evolution* **39**:8–23. DOI: https://doi.org/10.1111/j.1558-5646.1985.tb04076.x, PMID: 28563634

Bailey IW, Sinnott EW. 1916. The climatic distribution of certain types of angiosperm leaves. *American Journal of Botany* **3**:24–39. DOI: https://doi.org/10.1002/j.1537-2197.1916.tb05397.x

Bar M, Ori N. 2014. Leaf development and morphogenesis. *Development* **141**:4219–4230. DOI: https://doi.org/10.1242/dev.106195, PMID: 25371359

Barkoulas M, Hay A, Kougioumoutzi E, Tsiantis M. 2008. A developmental framework for dissected leaf formation in the *Arabidopsis* relative Cardamine hirsuta. *Nature Genetics* **40**:1136–1141. DOI: https://doi.org/10.1038/ng.189, PMID: 19165928

Berry J, Bjorkman O. 1980. Photosynthetic response and adaptation to temperature in higher plants. *Annual Review of Plant Physiology* **31**:491–543. DOI: https://doi.org/10.1146/annurev.pp.31.060180.002423

Bhikhi CR. 2011. Crepidospermum goudotianum (Tul.) Triana & Planch. https://data.biodiversitydata.nl/naturalis/specimen/U.1615275 [Accessed August 15, 2025].
Bilsborough GD, Runions A, Barkoulas M, Jenkins HW, Hasson A, Galinha C, Laufs P, Hay A, Prusinkiewicz P, Tsiantis M. 2011. Model for the regulation of *Arabidopsis thaliana* leaf margin development. *PNAS* **108**:3424–3429. DOI: https://doi.org/10.1073/pnas.1015162108, PMID: 21300866
Biviano MD, Jensen KH. 2025. Settling aerodynamics is a driver of symmetry in deciduous tree leaves. *Journal of The Royal Society Interface* **22**:20240654. DOI: https://doi.org/10.1098/rsif.2024.0654, PMID: 40328297
Blein T, Pulido A, Vialette-Guiraud A, Nikovics K, Morin H, Hay A, Johansen IE, Tsiantis M, Laufs P. 2008. A conserved molecular framework for compound leaf development. *Science* **322**:1835–1839. DOI: https://doi.org/10.1126/science.1166168, PMID: 19095941
Burnham RJ, Tonkovich GS. 2011. Climate, leaves, and the legacy of two giants. *New Phytologist* **190**:514–517. DOI: https://doi.org/10.1111/j.1469-8137.2011.03725.x, PMID: 21496027
Campitelli BE, Simonsen AK, Rico Wolf A, Manson JS, Stinchcombe JR. 2008. Leaf shape variation and herbivore consumption and performance: a case study with Ipomoea hederacea and three generalists. *Arthropod-Plant Interactions* **2**:9–19. DOI: https://doi.org/10.1007/s11829-007-9028-x
Campitelli BE, Stinchcombe JR. 2013a. Natural selection maintains a single-locus leaf shape cline in ivyleaf morning glory, Ipomoea hederacea. *Molecular Ecology* **22**:552–564. DOI: https://doi.org/10.1111/mec.12057, PMID: 23061399
Campitelli BE, Stinchcombe JR. 2013b. Testing potential selective agents acting on leaf shape in Ipomoea hederacea: predictions based on an adaptive leaf shape cline. *Ecology and Evolution* **3**:2409–2423. DOI: https://doi.org/10.1002/ece3.641
de Bruijn J. 1981. Kirengeshoma palmata Yatabe. https://data.biodiversitydata.nl/naturalis/specimen/WAG.1457187 [Accessed August 15, 2025].
Dell'Aglio DD, Losada ME, Jiggins CD. 2016. Butterfly learning and the diversification of plant leaf shape. *Frontiers in Ecology and Evolution* **4**:81. DOI: https://doi.org/10.3389/fevo.2016.00081
Dingle K, Camargo CQ, Louis AA. 2018. Input–output maps are strongly biased towards simple outputs. *Nature Communications* **9**:761. DOI: https://doi.org/10.1038/s41467-018-03101-6, PMID: 29472533
Donoghue MJ, Eaton DAR, Maya-Lastra CA, Landis MJ, Sweeney PW, Olson ME, Cacho NI, Moeglein MK, Gardner JR, Heaphy NM, Castorena M, Rivas AS, Clement WL, Edwards EJ. 2022. Replicated radiation of a plant clade along a cloud forest archipelago. *Nature Ecology & Evolution* **6**:1318–1329. DOI: https://doi.org/10.1038/s41559-022-01823-x, PMID: 35851851
Edwards EJ, Spriggs EL, Chatelet DS, Donoghue MJ. 2016. Unpacking a century-old mystery: winter buds and the latitudinal gradient in leaf form. *American Journal of Botany* **103**:975–978. DOI: https://doi.org/10.3732/ajb.1600129, PMID: 27221280
Ellis B, Daly D, Hickey L, Johnson K, Mitchell J, Wilf P, Wing S. 2009. *Manual of Leaf Architecture*. Cornell University Press. DOI: https://doi.org/10.1079/9781845935849.0000
Falster DS, Westoby M. 2003. Leaf size and angle vary widely across species: what consequences for light interception? *New Phytologist* **158**:509–525. DOI: https://doi.org/10.1046/j.1469-8137.2003.00765.x, PMID: 36056508
Felsenstein J. 1981. Evolutionary trees from DNA sequences: a maximum likelihood approach. *Journal of Molecular Evolution* **17**:368–376. DOI: https://doi.org/10.1007/BF01734359, PMID: 7288891
Foreman-Mackey D, Hogg DW, Lang D, Goodman J. 2013. Emcee: the MCMC Hammer . *Publications of the Astronomical Society of the Pacific* **125**:306–312. DOI: https://doi.org/10.1086/670067
Frye HA, Mocko K, Moore TE, Schlichting CD, Jones CS. 2020. Leaf margins in a deciduous lineage from the Greater Cape Floristic Region track climate in unexpected directions. *American Journal of Botany* **107**:735–748. DOI: https://doi.org/10.1002/ajb2.1472, PMID: 32399959
Geeta R, Dávalos LM, Levy A, Bohs L, Lavin M, Mummenhoff K, Sinha N, Wojciechowski MF. 2012. Keeping it simple: flowering plants tend to retain, and revert to, simple leaves. *New Phytologist* **193**:481–493. DOI: https://doi.org/10.1111/j.1469-8137.2011.03951.x, PMID: 22091556
Givnish TJ. 1987. Comparative studies of leaf form: assessing the relative roles of selective pressures and phylogenetic constraints. *New Phytologist* **106**:131–160. DOI: https://doi.org/10.1111/j.1469-8137.1987.tb04687.x
Givnish TJ, Kriebel R. 2017. Causes of ecological gradients in leaf margin entirety: evaluating the roles of biomechanics, hydraulics, vein geometry, and bud packing. *American Journal of Botany* **104**:354–366. DOI: https://doi.org/10.3732/ajb.1600287, PMID: 28232316
Hagolani PF, Zimm R, Vroomans R, Salazar-Ciudad I. 2021. On the evolution and development of morphological complexity: a view from gene regulatory networks. *PLOS Computational Biology* **17**:e1008570. DOI: https://doi.org/10.1371/journal.pcbi.1008570, PMID: 33626036
Higuchi Y, Kawakita A. 2019. Leaf shape deters plant processing by an herbivorous weevil. *Nature Plants* **5**:959–964. DOI: https://doi.org/10.1038/s41477-019-0505-x, PMID: 31477889
Janssens S, Couvreur TLP, Mertens A, Dauby G, Dagallier LP, Vanden Abeele S, Vandelook F, Mascarello M, Beeckman H, Sosef M, Droissart V, van der Bank M, Maurin O, Hawthorne W, Marshall C, Réjou-Méchain M, Beina D, Baya F, Merckx V, Verstraete B, et al. 2020. A large-scale species level dated angiosperm phylogeny for evolutionary and ecological analyses. *Biodiversity Data Journal*. DOI: https://doi.org/10.3897/BDJ.8.e39677
Johnston IG, Dingle K, Greenbury SF, Camargo CQ, Doye JPK, Ahnert SE, Louis AA. 2022. Symmetry and simplicity spontaneously emerge from the algorithmic nature of evolution. *PNAS* **119**:e2113883119. DOI: https://doi.org/10.1073/pnas.2113883119, PMID: 35275794

Kalbfleisch JD, Lawless JF. 1985. The analysis of panel data under a Markov assumption. *Journal of the American Statistical Association* **80**:863–871. DOI: https://doi.org/10.1080/01621459.1985.10478195
Kavanagh KD, Shoval O, Winslow BB, Alon U, Leary BP, Kan A, Tabin CJ. 2013. Developmental bias in the evolution of phalanges. *PNAS* **110**:18190–18195. DOI: https://doi.org/10.1073/pnas.1315213110, PMID: 24151335
Kidner CA, Umbreen S. 2010. Why is leaf shape so variable?. *International Journal of Plant Developmental Biology* **4**:64–75.
Kierzkowski D, Runions A, Vuolo F, Strauss S, Lymbouridou R, Routier-Kierzkowska AL, Wilson-Sánchez D, Jenke H, Galinha C, Mosca G, Zhang Z, Canales C, Dello Ioio R, Huijser P, Smith RS, Tsiantis M. 2019. A growth-based framework for leaf shape development and diversity. *Cell* **177**:1405–1418. DOI: https://doi.org/10.1016/j.cell.2019.05.011, PMID: 31130379
Kirchoff BK. 2003. Shape matters: Hofmeister's rule, primordium shape, and flower orientation. *International Journal of Plant Sciences* **164**:505–517. DOI: https://doi.org/10.1086/375421
Koenig D, Bayer E, Kang J, Kuhlemeier C, Sinha N. 2009. Auxin patterns Solanum lycopersicum leaf morphogenesis. *Development* **136**:2997–3006. DOI: https://doi.org/10.1242/dev.033811, PMID: 19666826
Kuchen EE, Fox S, Barbier de Reuille P, Kennaway R, Bensmihen S, Avondo J, Calder GM, Southam P, Robinson S, Bangham A, Coen E. 2012. Generation of leaf shape through early patterns of growth and tissue polarity. *Science* **335**:1092–1096. DOI: https://doi.org/10.1126/science.1214678, PMID: 22383846
Laland K, Uller T, Feldman M, Sterelny K, Müller GB, Moczek A, Jablonka E, Odling-Smee J, Wray GA, Hoekstra HE, Futuyma DJ, Lenski RE, Mackay TFC, Schluter D, Strassmann JE. 2014. Does evolutionary theory need a rethink? *Nature* **514**:161–164. DOI: https://doi.org/10.1038/514161a, PMID: 25297418
Leigh A, Sevanto S, Close JD, Nicotra AB. 2017. The influence of leaf size and shape on leaf thermal dynamics: does theory hold up under natural conditions? *Plant, Cell & Environment* **40**:237–248. DOI: https://doi.org/10.1111/pce.12857, PMID: 28026874
Li Y, Wang Z, Xu X, Han W, Wang Q, Zou D. 2016. Leaf margin analysis of Chinese woody plants and the constraints on its application to palaeoclimatic reconstruction. *Global Ecology and Biogeography* **25**:1401–1415. DOI: https://doi.org/10.1111/geb.12498
Little SA, Kembel SW, Wilf P. 2010. Paleotemperature proxies from leaf fossils reinterpreted in light of evolutionary history. *PLOS ONE* **5**:e15161. DOI: https://doi.org/10.1371/journal.pone.0015161, PMID: 21203554
Louf JF, Nelson L, Kang H, Song PN, Zehnbauer T, Jung S. 2018. How wind drives the correlation between leaf shape and mechanical properties. *Scientific Reports* **8**:16314. DOI: https://doi.org/10.1038/s41598-018-34588-0, PMID: 30397247
Malone J. 2026. Leaf-shape-evolution. swh:1:rev:ed207598f0023c617b2c950193fc9179e94abff2. Software Heritage. https://archive.softwareheritage.org/swh:1:dir:337904c1feefe422049b09f412e159e6dbb478cd;origin=https://github.com/malonej501/leaf-shape-evolution;visit=swh:1:snp:8153a1fcf866735ed249133e87d3fc04ea14923e;anchor=swh:1:rev:ed207598f0023c617b2c950193fc9179e94abff2
Martin NS, Camargo CQ, Louis AA. 2024. Bias in the arrival of variation can dominate over natural selection in Richard Dawkins's biomorphs. *PLOS Computational Biology* **20**:e1011893. DOI: https://doi.org/10.1371/journal.pcbi.1011893, PMID: 38536880
McGibbon RT, Pande VS. 2015. Efficient maximum likelihood parameterization of continuous-time Markov processes. *The Journal of Chemical Physics* **143**:034109. DOI: https://doi.org/10.1063/1.4926516, PMID: 26203016
Meade A, Pagel M. 2024. BayesTraits manual. Version 4.1.2. BayesTraits. https://www.evolution.reading.ac.uk/BayesTraitsV4.1.2/BayesTraitsV4.1.2.html
Naturalis Biodiversity Center. 2024. Naturalis Bioportal. https://bioportal.naturalis.nl [Accessed August 15, 2025].
Nicotra AB, Leigh A, Boyce CK, Jones CS, Niklas KJ, Royer DL, Tsukaya H. 2011. The evolution and functional significance of leaf shape in the angiosperms. *Functional Plant Biology* **38**:535–552. DOI: https://doi.org/10.1071/FP11057, PMID: 32480907
Niklas K. 1996. Differences between Acer saccharum leaves from open and wind-protected sites. *Annals of Botany* **78**:61–66. DOI: https://doi.org/10.1006/anbo.1996.0096
Niklas KJ. 1999. A mechanical perspective on foliage leaf form and function. *New Phytologist* **143**:19–31. DOI: https://doi.org/10.1046/j.1469-8137.1999.00441.x
Niklas KJ, Cobb ED, Niinemets Ü, Reich PB, Sellin A, Shipley B, Wright IJ. 2007. "Diminishing returns" in the scaling of functional leaf traits across and within species groups. *PNAS* **104**:8891–8896. DOI: https://doi.org/10.1073/pnas.0701135104, PMID: 17502616
Nikolov LA, Runions A, Das Gupta M, Tsiantis M. 2019. Leaf development and evolution. In: Grossniklaus U (Ed). *Current Topics in Developmental Biology*. Elsevier. p. 109–139. DOI: https://doi.org/10.1016/bs.ctdb.2018.11.006
Otto D, Munz S, Memic E, Hartung J, Graeff-Hönninger S. 2025. A computer vision approach for quantifying leaf shape of maize (Zea mays L.) and simulating its impact on light interception. *Frontiers in Plant Science* **16**:1521242. DOI: https://doi.org/10.3389/fpls.2025.1521242, PMID: 40625874
Pagel M. 1994. Detecting correlated evolution on phylogenies: a general method for the comparative analysis of discrete characters. *Proceedings of the Royal Society of London. Series B* **255**:37–45. DOI: https://doi.org/10.1098/rspb.1994.0006

Pagel M, Meade A, Barker D. 2004. Bayesian estimation of ancestral character states on phylogenies. *Systematic Biology* **53**:673–684. DOI: https://doi.org/10.1080/10635150490522232, PMID: 15545248

Pagel M, O'Donovan C, Meade A. 2022. General statistical model shows that macroevolutionary patterns and processes are consistent with Darwinian gradualism. *Nature Communications* **13**:1113. DOI: https://doi.org/10.1038/s41467-022-28595-z, PMID: 35236836

Peppe DJ, Royer DL, Cariglino B, Oliver SY, Newman S, Leight E, Enikolopov G, Fernandez-Burgos M, Herrera F, Adams JM, Correa E, Currano ED, Erickson JM, Hinojosa LF, Hoganson JW, Iglesias A, Jaramillo CA, Johnson KR, Jordan GJ, Kraft NJB, et al. 2011. Sensitivity of leaf size and shape to climate: global patterns and paleoclimatic applications. *New Phytologist* **190**:724–739. DOI: https://doi.org/10.1111/j.1469-8137.2010.03615.x, PMID: 21294735

Perez RPA, Dauzat J, Pallas B, Lamour J, Verley P, Caliman JP, Costes E, Faivre R. 2018. Designing oil palm architectural ideotypes for optimal light interception and carbon assimilation through a sensitivity analysis of leaf traits. *Annals of Botany* **121**:909–926. DOI: https://doi.org/10.1093/aob/mcx161, PMID: 29293866

Perez TM, Feeley KJ. 2020. Photosynthetic heat tolerances and extreme leaf temperatures. *Functional Ecology* **34**:2236–2245. DOI: https://doi.org/10.1111/1365-2435.13658

Perico C, Tan S, Langdale JA. 2022. Developmental regulation of leaf venation patterns: monocot versus eudicots and the role of auxin. *New Phytologist* **234**:783–803. DOI: https://doi.org/10.1111/nph.17955, PMID: 35020214

Plowman TC. 1981. Erythroxylum confusum Britton. https://data.biodiversitydata.nl/naturalis/specimen/U.1284618 [Accessed August 15, 2025].

Prusinkiewicz P, Erasmus Y, Lane B, Harder LD, Coen E. 2007. Evolution and development of inflorescence architectures. *Science* **316**:1452–1456. DOI: https://doi.org/10.1126/science.1140429, PMID: 17525303

Rausher MD. 1978. Search image for leaf shape in a butterfly. *Science* **200**:1071–1073. DOI: https://doi.org/10.1126/science.200.4345.1071, PMID: 17740703

Roden JS, Pearcy RW. 1993a. Effect of leaf flutter on the light environment of poplars. *Oecologia* **93**:201–207. DOI: https://doi.org/10.1007/BF00317672, PMID: 28313608

Roden JS, Pearcy RW. 1993b. Photosynthetic gas exchange response of poplars to steady-state and dynamic light environments. *Oecologia* **93**:208–214. DOI: https://doi.org/10.1007/BF00317673, PMID: 28313609

Roden JS. 2003. Modeling the light interception and carbon gain of individual fluttering aspen (Populus tremuloides Michx) leaves. *Trees* **17**:117–126. DOI: https://doi.org/10.1007/s00468-002-0213-3

Rohner PT, Berger D. 2023. Developmental bias predicts 60 million years of wing shape evolution. *PNAS* **120**:e2211210120. DOI: https://doi.org/10.1073/pnas.2211210120, PMID: 37126721

Royer DL, Wilf P, Janesko DA, Kowalski EA, Dilcher DL. 2005. Correlations of climate and plant ecology to leaf size and shape: potential proxies for the fossil record. *American Journal of Botany* **92**:1141–1151. DOI: https://doi.org/10.3732/ajb.92.7.1141, PMID: 21646136

Royer DL, Wilf P. 2006. Why do toothed leaves correlate with cold climates? Gas exchange at leaf margins provides new insights into a classic paleotemperature proxy. *International Journal of Plant Sciences* **167**:11–18. DOI: https://doi.org/10.1086/497995

Royer DL, Peppe DJ, Wheeler EA, Niinemets Ü. 2012. Roles of climate and functional traits in controlling toothed vs. untoothed leaf margins. *American Journal of Botany* **99**:915–922. DOI: https://doi.org/10.3732/ajb.1100428, PMID: 22494908

Runions A, Tsiantis M, Prusinkiewicz P. 2017. A common developmental program can produce diverse leaf shapes. *New Phytologist* **216**:401–418. DOI: https://doi.org/10.1111/nph.14449, PMID: 28248421

Sack L, Frole K. 2006. Leaf structural diversity is related to hydraulic capacity in tropical rain forest trees. *Ecology* **87**:483–491. DOI: https://doi.org/10.1890/05-0710, PMID: 16637372

Sack L, Scoffoni C. 2013. Leaf venation: structure, function, development, evolution, ecology and applications in the past, present and future. *New Phytologist* **198**:983–1000. DOI: https://doi.org/10.1111/nph.12253, PMID: 23600478

Scarpella E, Marcos D, Friml J, Berleth T. 2006. Control of leaf vascular patterning by polar auxin transport. *Genes & Development* **20**:1015–1027. DOI: https://doi.org/10.1101/gad.1402406, PMID: 16618807

Scarpella E, Barkoulas M, Tsiantis M. 2010. Control of leaf and vein development by auxin. *Cold Spring Harbor Perspectives in Biology* **2**:a001511. DOI: https://doi.org/10.1101/cshperspect.a001511, PMID: 20182604

Scarpella E. 2024. Leaf vein patterning. *Annual Review of Plant Biology* **75**:377–398. DOI: https://doi.org/10.1146/annurev-arplant-062923-030348, PMID: 38382907

Scoffoni C, Rawls M, McKown A, Cochard H, Sack L. 2011. Decline of leaf hydraulic conductance with dehydration: relationship to leaf size and venation architecture. *Plant Physiology* **156**:832–843. DOI: https://doi.org/10.1104/pp.111.173856, PMID: 21511989

Singhal YK, Boyle JA, Stinchcombe JR. 2025. Differences in stomatal conductance between leaf shape genotypes of *Ipomoea hederacea* suggest divergent ecophysiological strategies. *bioRxiv*. DOI: https://doi.org/10.1101/2025.02.01.636047

Sisó S, Camarero JJ, Gil-Pelegrín E. 2001. Relationship between hydraulic resistance and leaf morphology in broadleaf Quercus species: a new interpretation of leaf lobation. *Trees* **15**:341–345. DOI: https://doi.org/10.1007/s004680100110

Smith JM, Burian R, Kauffman S, Alberch P, Campbell J, Goodwin B, Lande R, Raup D, Wolpert L. 1985. Developmental constraints and evolution: a perspective from the mountain lake conference on development and evolution. *The Quarterly Review of Biology* **60**:265–287. DOI: https://doi.org/10.1086/414425

Soltis D. 2000. Angiosperm phylogeny inferred from 18S rDNA, rbcL, and atpB sequences. *Botanical Journal of the Linnean Society* **133**:381–461. DOI: https://doi.org/10.1006/bojl.2000.0380
Staps M, Miller PW, Tarnita CE, Mallarino R. 2023. Development shapes the evolutionary diversification of rodent stripe patterns. *PNAS* **120**:e2312077120. DOI: https://doi.org/10.1073/pnas.2312077120, PMID: 37871159
Tadrist L, Darbois-Texier B. 2016. Are leaves optimally designed for self-support? An investigation on giant monocots. *Journal of Theoretical Biology* **396**:125–131. DOI: https://doi.org/10.1016/j.jtbi.2016.02.018, PMID: 26920248
The Angiosperm Phylogeny Group. 2016. An update of the Angiosperm Phylogeny Group classification for the orders and families of flowering plants: APG IV. *Botanical Journal of the Linnean Society* **181**:1–20. DOI: https://doi.org/10.1111/boj.12385
Uller T, Moczek AP, Watson RA, Brakefield PM, Laland KN. 2018. Developmental bias and evolution: a regulatory network perspective. *Genetics* **209**:949–966. DOI: https://doi.org/10.1534/genetics.118.300995, PMID: 30049818
van Nimwegen E, Crutchfield JP, Huynen M. 1999. Neutral evolution of mutational robustness. *PNAS* **96**:9716–9720. DOI: https://doi.org/10.1073/pnas.96.17.9716, PMID: 10449760
van Royen P. 1973. Geranium caespitosum E. James. https://data.biodiversitydata.nl/naturalis/specimen/L.2011772 [Accessed August 15, 2025].
Vlad D, Kierzkowski D, Rast MI, Vuolo F, Dello Ioio R, Galinha C, Gan X, Hajheidari M, Hay A, Smith RS, Huijser P, Bailey CD, Tsiantis M. 2014. Leaf shape evolution through duplication, regulatory diversification, and loss of a homeobox gene. *Science* **343**:780–783. DOI: https://doi.org/10.1126/science.1248384, PMID: 24531971
Vogel S. 1970. Convective cooling at low airspeeds and the shapes of broad leaves. *Journal of Experimental Botany* **21**:91–101. DOI: https://doi.org/10.1093/jxb/21.1.91
Vogel S. 1989. Drag and reconfiguration of broad leaves in high winds. *Journal of Experimental Botany* **40**:941–948. DOI: https://doi.org/10.1093/jxb/40.8.941
von der Dunk SHA, Martin NS, Dingle K, Louis AA. 2025 RNA secondary structures are conserved but random. *bioRxiv*. DOI: https://doi.org/10.1101/2025.08.18.670923
Watson DJ. 1958. The dependence of net assimilation rate on leaf-area index. *Annals of Botany* **22**:37–54. DOI: https://doi.org/10.1093/oxfordjournals.aob.a083596
Welch JJ. 2017. What's wrong with evolutionary biology? *Biology & Philosophy* **32**:263–279. DOI: https://doi.org/10.1007/s10539-016-9557-8, PMID: 28298744
Wolfe JA. 1993. *A Method of Obtaining Climatic Parameters from Leaf Assemblages*. U.S. Government Printing Office.
Wright IJ, Reich PB, Westoby M, Ackerly DD, Baruch Z, Bongers F, Cavender-Bares J, Chapin T, Cornelissen JHC, Diemer M, Flexas J, Garnier E, Groom PK, Gulias J, Hikosaka K, Lamont BB, Lee T, Lee W, Lusk C, Midgley JJ, et al. 2004. The worldwide leaf economics spectrum. *Nature* **428**:821–827. DOI: https://doi.org/10.1038/nature02403, PMID: 15103368
Wright IJ, Dong N, Maire V, Prentice IC, Westoby M, Díaz S, Gallagher RV, Jacobs BF, Kooyman R, Law EA, Leishman MR, Niinemets Ü, Reich PB, Sack L, Villar R, Wang H, Wilf P. 2017. Global climatic drivers of leaf size. *Science* **357**:917–921. DOI: https://doi.org/10.1126/science.aal4760, PMID: 28860384
Zimm R, Berio F, Debiais-Thibaud M, Goudemand N. 2023. A shark-inspired general model of tooth morphogenesis unveils developmental asymmetries in phenotype transitions. *PNAS* **120**:e2216959120. DOI: https://doi.org/10.1073/pnas.2216959120, PMID: 37027430
Zimmermann W. 1952. Main results of the "Telome Theory". *The Palaeobotanist* **1**:456–470. DOI: https://doi.org/10.54991/jop.1952.423
Zohner CM, Ramm E, Renner SS. 2019. Examining the support-supply and bud-packing hypotheses for the increase in toothed leaf margins in northern deciduous floras. *American Journal of Botany* **106**:1404–1411. DOI: https://doi.org/10.1002/ajb2.1379, PMID: 31670844
Zuntini AR, Carruthers T. 2024. Phylogenomics and the rise of the angiosperms. *Zenodo*. DOI: https://doi.org/10.5281/zenodo.10778206
Zuntini AR, Carruthers T, Maurin O, Bailey PC, Leempoel K, Brewer GE, Epitawalage N, Françoso E, Gallego-Paramo B, McGinnie C, Negrão R, Roy SR, Simpson L, Toledo Romero E, Barber VMA, Botigué L, Clarkson JJ, Cowan RS, Dodsworth S, Johnson MG, et al. 2024. Phylogenomics and the rise of the angiosperms. *Nature* **629**:843–850. DOI: https://doi.org/10.1038/s41586-024-07324-0

Appendix 1

Extended data

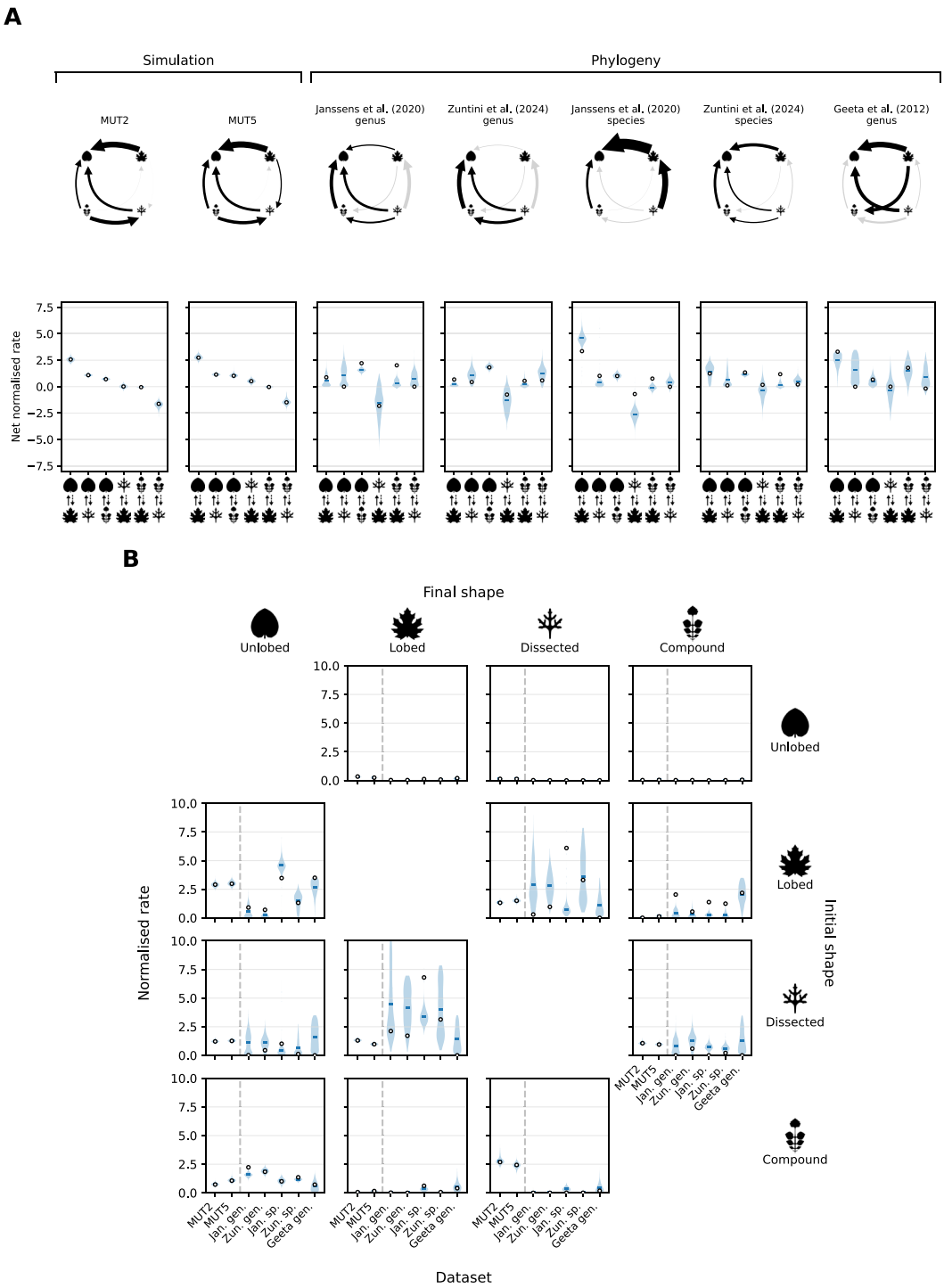

Appendix 1—figure 1. Further details of transition rates from phylogenies and simulations. (**A**) Net normalised transition rates between the four leaf shape categories, inferred from both simulation and phylogeny. (Top row) Arrow thickness and direction represent the mean net normalised transition rate between each pair of leaf shape categories. Black arrows represent transitions where 0 does not fall within an equal-tailed 95% credible interval for the net normalised posterior, and grey where it does. (Bottom row) Posterior distributions for the net

Appendix 1—figure 1 continued on next page

Appendix 1—figure 1 continued

normalised rate of all transitions. Solid bars indicate the mean and circular points represent MLE estimates. The net rate is calculated by subtracting the transition given by the dashed arrow from the transition given by the solid arrow in the x-axis labels. (**B**) Normalised transition rates between different leaf shapes, inferred from both in silico mutagenesis (left of dashed line) and phylogeny (right of dashed line). Each subplot represents a different transition, from the shape shown on the vertical figure axis to the shape shown on the horizontal figure axis. These rates were normalised by dividing by the mean transition rate estimate within each dataset (***Equation 6***).

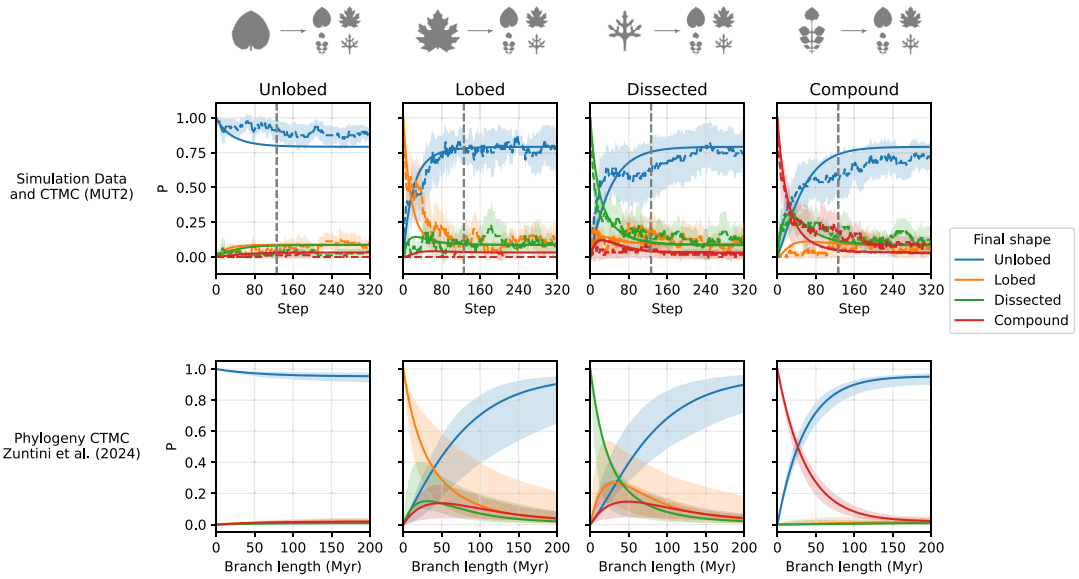

Appendix 1—figure 2. Comparing in silico mutagenesis and phylogeny for the probability of each shape transition over time, separated out by starting shape. The column header gives the initial shape and the line colour gives the final shape. (Top row) The dashed line represents the proportion of walks from each unique initial leaf (***Appendix 2—figure 6***), averaged over all initial leaves in each state. The error bands represent $\pm 1.96\times$ standard error for this average. The solid lines represent the CTMC model fit (MLE) to the output of the random walks. The vertical, grey, dashed line represents the estimated simulation step that is equivalent to $t = 200$ Myr for the phylogeny CTMC. This is calculated as described in ***Figure 3***, and is also the simulation x-limit in ***Figure 3***. We show all 320 simulation steps here for a more detailed summary of the simulation trajectories. (Bottom row) The predicted transition probabilities given by the CTMC model fit to the labelled ***Zuntini et al., 2024*** genus tree (***Figure 1—figure supplement 2***). The solid line represents the MLE fit and the errors are inferred from MCMC posteriors via Monte Carlo error propagation (N = 500) as per ***Figure 3***. Note the good qualitative agreement between the phylogenetic and simulation dynamics, especially for the (blue) data related to transitions to/from unlobed leaves.

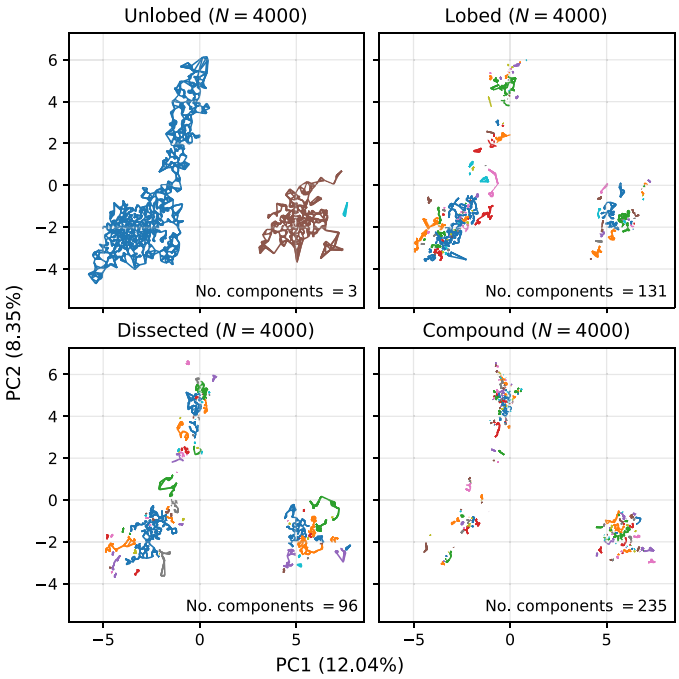

Appendix 1—figure 3. The nearest neighbour graph of parameter PCA space for each shape category highlights how the unlobed space is the most connected, followed by dissected, lobed, and then compound. Complex leaves subdivide into many more connected components than unlobed. This pattern is also observed when the nearest-neighbour graph is constructed in the full-dimensional parameter space, where the numbers of connected components are 146, 273, 255, and 315 for unlobed, lobed, dissected, and compound leaves, respectively. Thus, the greater connectedness of the unlobed parameter space is not an artefact of the PCA projection. The number of nearest neighbours used is 6. Colours highlight different connected components; however, since the number of unique colours is only 10, this under-represents the true number of connected components for lobed, dissected, and compound. Thus, the colours here are intended only as a visual guide.

Appendix 2

Extended simulation methods

Leaf model details

In this section, we provide a more detailed overview of how model parameters relate to growth processes. For further model details, please also see the main text and supplementary information of ***Runions et al., 2017***.

Initialisation

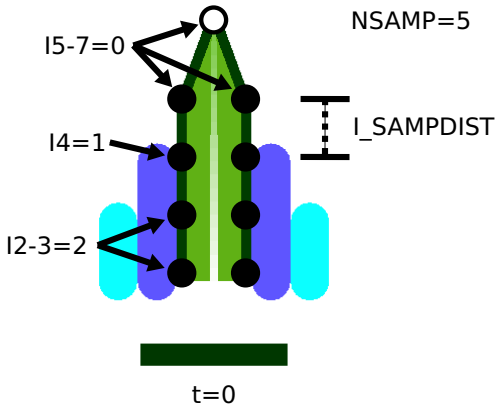

Appendix 2—figure 1. The initial leaf 'primordium' at the start of the simulation labelled with a selection of initialisation parameters. Parameters I0–I12 specify which compounds/morphogens are present at each sample point, in this case either compound 0, 1 or 2. I_SAMPDIST specifies the vertical distance between sample points and NSAMP gives the total primordium length in number of sample points.

The initial condition of the ***Runions et al., 2017*** simulation is a primordium (***Appendix 2—figure 1***) with user-defined dimensions and morphogen distribution along the margin. These properties are specified by the following initialisation parameters.

- NSAMP – primordium length in number of sample points.
- I_SAMPDIST – vertical distance between sample points.
- INITSTATE – an array containing I0–I12. Specifies which compounds are present at each sample point in the primordium.
- PRIMSCALEX – the primordium is scaled in x according to this value.
- PRIMSCALEY – the primordium is scaled in y according to this value.

Margin webbing

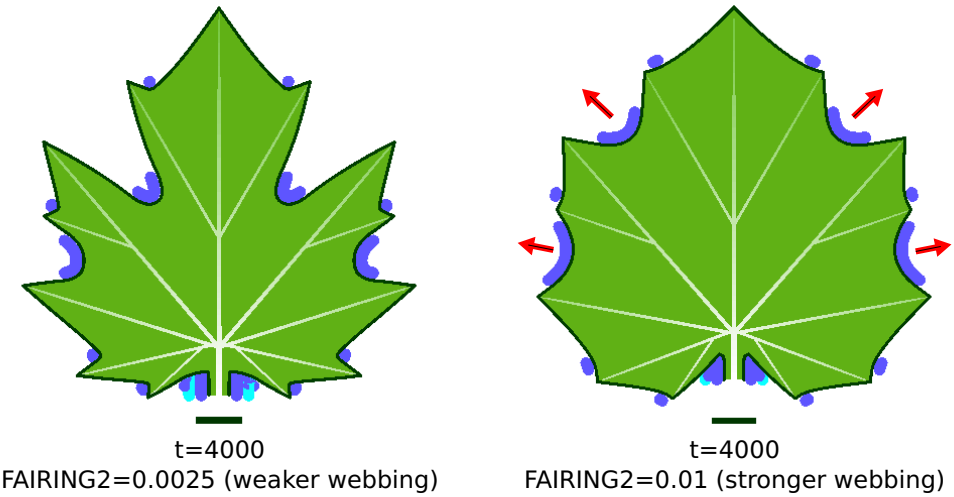

Appendix 2—figure 2. Stronger webbing results in shallower lobes. Stronger webbing results in faster growth of the margin and lamina between vein tips (convergence points) to reduce stretching. The overall rate of webbing depends on multiple morphogen-associated model parameters. In this example, compound 2 (dark blue) has stronger webbing for the right-hand leaf, resulting in faster growth in the lobes where it is localised.

The margin parameters control patterning, webbing and tip growth. Patterning is the addition of new vein tips (convergence points) and the updating of compound positions. Webbing is the rate at which the margin deforms to reduce stretching and bending. Tip growth is the rate of extension of vein tips.

Webbing (***Appendix 2—figure 2***) is simulated for each sample point $\boldsymbol{P_i}$ along the leaf margin that is not a vein tip/convergence point, where i is the sample point index. It is implemented as a displacement vector $\Delta \boldsymbol{W_i}$ that is calculated as the weighted sum of 4 other displacement vectors: stretch ($\Delta \boldsymbol{S_i}$), curvature 1 ($\Delta \boldsymbol{K_i^{(1)}}$), curvature 2 ($\Delta \boldsymbol{K_i^{(2)}}$), and normal displacement ($\boldsymbol{N_i}$).

$$\Delta \boldsymbol{W_i} = \alpha_S \Delta \boldsymbol{S_i} + \alpha_{K^{(1)}} \Delta \boldsymbol{K_i^{(1)}} + \alpha_{K^{(2)}} \Delta \boldsymbol{K_i^{(2)}} + \alpha_N \boldsymbol{N_i} \tag{2.1}$$

Each of these vectors is weighted by user-controlled parameters α_S, $\alpha_{K^{(1)}}$, $\alpha_{K^{(2)}}$ and α_N. The first three vectors ($\Delta \boldsymbol{S_i}$, $\Delta \boldsymbol{K_i^{(1)}}$, $\Delta \boldsymbol{K_i^{(2)}}$) are calculated by minimising an energy term for all sample points in the margin $\boldsymbol{P_0}, \boldsymbol{P_1}, ..., \boldsymbol{P_n}$.

The stretch energy E_S is given by

$$E_S = \sum_{i=1}^{n} \|\boldsymbol{P_i} - \boldsymbol{P_{i-1}}\|^2. \tag{2.2}$$

Curvature is approximated using two different expressions for additional flexibility. The first curvature energy is approximated for each sample point by the turning angle θ_i. So for the entire margin this results in the curvature energy

$$E_{K^{(1)}} = \sum_{i=1}^{n-1} \theta_i^2. \tag{2.3}$$

The second curvature energy is given by the weighted second finite difference about each sample point

$$E_{K^{(2)}} = \sum_{i=1}^{n-1} \|w_l^i \boldsymbol{P_{i-1}} - w_c^i \boldsymbol{P_i} + w_r^i \boldsymbol{P_{i+1}}\|^2, \tag{2.4}$$

where $w_l^i = w_r^i = \frac{1}{2}$ and $w_c^i = 1$. These weights result in a vector from $\boldsymbol{P_i}$ to the mid-point of the line between $\boldsymbol{P_{i-1}}$ and $\boldsymbol{P_{i+1}}$.

Finally the magnitude of the normal displacement vector for each sample point $\boldsymbol{P_i}$ is proportional to the average length of the adjacent margin edges

$$\frac{1}{2}\left(\|\boldsymbol{P_{i+1}} - \boldsymbol{P_i}\| + \|\boldsymbol{P_i} - \boldsymbol{P_{i-1}}\|\right). \tag{2.5}$$

To calculate the overall webbing vector for each sample point, each of these terms is weighted by a user-controlled parameter: stretch (α_S) - STRETCH, curvature 1 ($\alpha_{K^{(1)}}$) - CFLOW, curvature 2 ($\alpha_{K^{(2)}}$) - CURVATURE, normal displacement (α_N) - NORMAL.

Many margin parameters are associated with particular morphogens/compounds and have the name format `<parameter_name><morphogen_number>`, e.g. FAIRING2. For a particular margin segment, not all margin parameters are necessarily used, as the parameters used depend on the compounds present there. If there are 2 compounds present, each will have its own set of parameters actively playing a role in growth and form. Webbing can be controlled by the user via the following parameters.

- TIP_GROWTH – controls the rate at which vein tips are displaced in the vein direction.
- FAIRING – controls the total rate of webbing.
- CURVATURE – controls the rate of bending.
- CFLOW – controls the rate of bending.
- STRETCH – controls the distance between neighbouring margin points.
- NORMAL – the amount that margin points are displaced normal to the curve.

Margin patterning

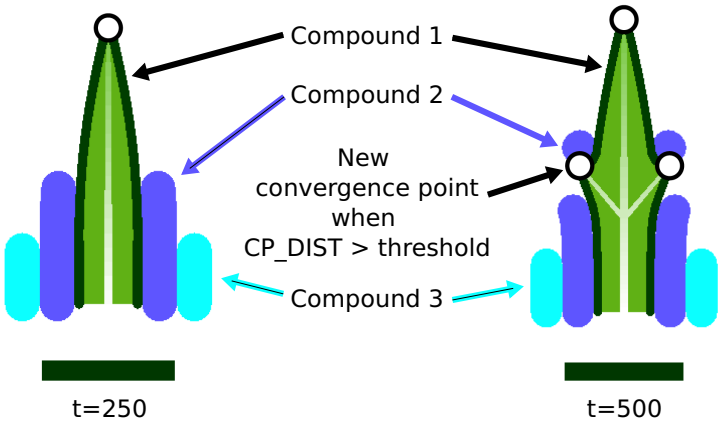

Appendix 2—figure 3. Margins are patterned by convergence points and morphogens/compounds. New convergence points are inserted between existing convergence points, where the intervening distance along the margin exceeds a threshold value. Compounds/morphogens on the margin can alter the measured distances between convergence points, affecting where new convergence points are inserted. New veins are inserted to connect new convergence points to the existing vasculature, thereby specifying new growth axes. Compounds can also alter the rate of webbing between veins.

The margin is patterned by convergence points, which mark the tips of new veins, and compounds (also referred to as morphogens) (***Appendix 2—figure 3***). The patterning process occurs by first measuring distances along the margin. This informs where convergence points and thus veins should be added. The margin points at which compounds are expressed are updated in response to the new convergence points. Finally, new veins are added to connect the convergence points to the existing vasculature.

The following parameters control margin patterning globally.

- LASSYMETRY – the distance value on the first (left) point along the margin. Can be thought of as the effect of neighbouring tissue on the leaf primordium.
- RASSYMETRY – the distance value on the last (right) point along the margin.
- INTERVAL – the distance along the margin between two convergence points over which a compound will be expressed.

The following parameters have compound-specific effects.

- METRIC – the rate at which distances along the margin increase relative to arc-length distances. Measured distances can increase more slowly or more rapidly than the arc-length distance as the leaf grows depending on the value here.
- CPDIST – new convergence points are added to a margin segment when the distance measured along this segment exceeds this value. This may differ between compounds.
- PATTERNABLE – controls whether margin segments expressing this compound are competent for new convergence points.
- COMPETENCE – sets the maximum distance from the leaf base a margin segment can be and still be competent for new convergence points.
- COMPETENCET – maximum time step beyond which a margin segment will no longer be competent for new convergence points.
- EXTENDABLE – whether the interval in which a compound is expressed can increase in size or not.
- EXTENDABLE_CONTEXT – which compounds can be overwritten. When a compound number is greater than this value, it can be overwritten.

Vein patterning

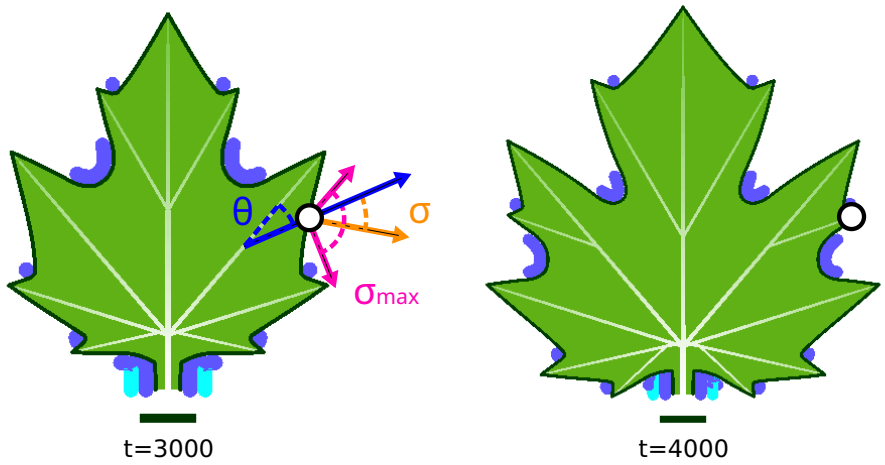

Appendix 2—figure 4. New veins attach to existing vasculature at angle θ. Attachment is restricted such that the angle made with the margin σ cannot exceed σ_{max}. Veins attach so as to minimise 'resistance'—the total distance from the vein tip to either the base of the leaf or the existing vasculature, depending on the value of GLOBAL_RESISTANCE.

New veins attach convergence points to existing vasculature so as to minimise resistance (***Appendix 2—figure 4***). Resistance depends on the distance travelled in the blade and the distance travelled in the vasculature to the leaf base. The user can exert some control over vein attachment through the following parameters.

- AXISANGLE – the angle at which new veins branch from existing veins.
- MAXANGLE – the maximum angle veins can make with the margin. This restricts the orientation of new veins.
- GLOBAL_RESISTANCE – determines how the resistance (length) of veins affects where a vein will join to the existing vasculature. A value of 0 means only the resistance of the new vein

segment is considered. A value of 1 means the total resistance of the entire path to the leaf base is considered.

Global growth

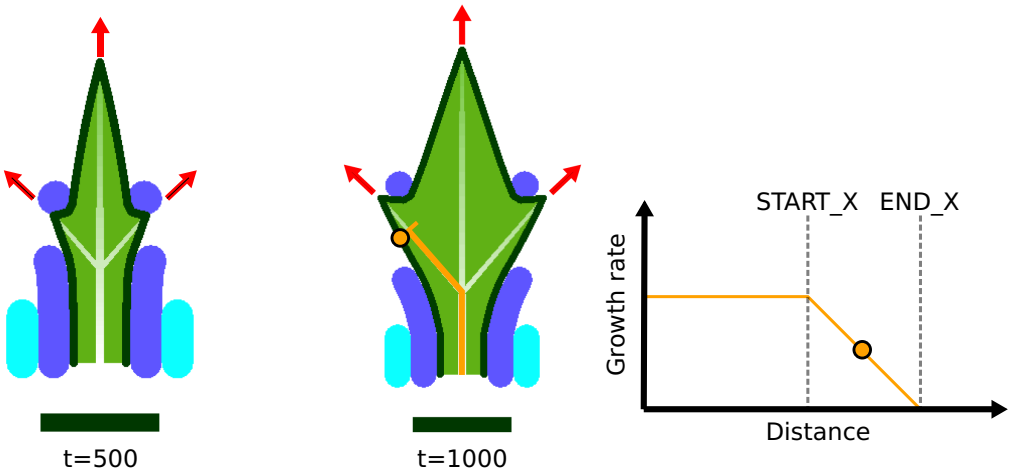

Appendix 2—figure 5. Veins are the main axes of growth, pushing the local margin outwards in successive time points. The rate of growth of the veins and margin depends on the distance to the base of the leaf. Growth of veins and margin is fastest near the base of the leaf, tailing off towards the tip depending on the values of parameters such as VG_START_X for vein growth.

Growth is a combination of uniform scaling, vein tip displacement, webbing and vein extension. The global rate of tip displacement, webbing and vein extension depends on the distance to the leaf base as measured along the veins according to a growth gradient (***Appendix 2—figure 5***). Vein growth rate can also be age-dependent.

- UNIFORM_GROWTH – the rate of uniform scaling.
- TG_START_X – the distance from the leaf base along the veins that the rate of tip growth begins to decrease.
- TG_END_X – the distance from the leaf base along the veins that the rate of tip growth reaches its minimum.
- FG_START_X – the distance from the leaf base that the rate of webbing growth begins to fall off.
- FG_END_X – the distance from the leaf base that the rate of webbing growth stops decreasing.
- VG_GRATE – base vein growth rate.
- VG_START_X – distance from leaf base that the rate of vein growth begins to fall off.
- VG_END_X – distance from leaf base that the rate of vein growth stops decreasing.
- CP_AD_TIP_GROWTH – rate of extra early tip growth.
- CP_ADTG_FALLOFF – time period over which early growth disappears.
- AX_AD_AXIS_GROWTH – rate of extra early vein-extension.
- AX_ADAG_FALLOFF – time period over which early vein extension growth disappears.

Miscellaneous

- APEX_TIP_GROWTH – extra tip growth for the primary axis.
- ASYMMETRIC_FAIRING – whether the rate of webbing can be different on either side of a convergence point.
- ASYMM_PRE – the rate of webbing before the convergence point.
- ASYMM_POST – the rate of webbing after the convergence point.
- SHARP_LEAF_TIP – whether to disable webbing at the leaf tip.
- INTERNAL_FLOW – whether webbing can only occur in the outward direction.
- PETIOLE_COMPOUND – the compound which specifies the petiole.

- PETIOLE_EXTEND – whether the petiole (as marked by PETIOLE_COMPOUND) is enlarged by uniform growth.

Initial leaves

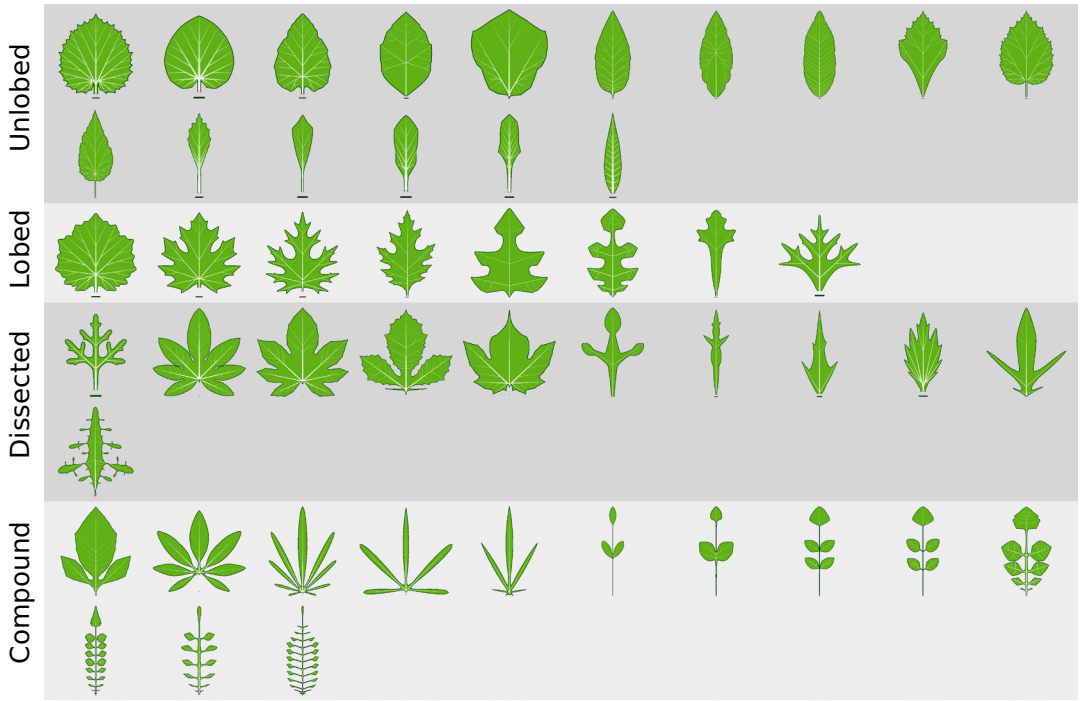

Appendix 2—figure 6. The sample of 48 leaves used as the starting points for random walks. 16 unlobed (u), 8 lobed (l), 11 dissected (d), and 13 compound (c).

All random walk algorithms

Appendix 2 —algorithm 2.1: Random Walk MUT2

```
θ ← initial parameter values
for step ← 0 to N_maxGenerated − 1 do
    for attempt ← 0 to N_maxAttempts − 1 do
        θ′ ← θ                                          // Copy parameters for this
        step
        mutation ← random draw from {
          uniform[0.1,1),
          uniform[1,10),
          uniform[10,100)
        }
        sign ← random choice from {−1, 1}
        i ← random draw from {0,…,length(θ)−1}
        θ′[i] ← θ[i] + (mutation × sign)                // Mutate
        Run simulation with θ′
        if leaf passes sanity checks then
            θ ←θ′                                       // Save new parameters
            break
```

Appendix 2 — algorithm 2.2: Random Walk MUT5

```
θ ← initial parameter values
for step ← 0 to N_maxGenerated − 1 do
    for attempt ← 0 to N_maxAttempts − 1 do
        θ′ ← θ                                              // Copy parameters for
        this step
        mutation ← random draw from {
          uniform[0.1, 1),
          uniform[1, 10),
          uniform[10, 100)
        }
        sign ← random choice from {−1, 1}
        scale ← 0.1 × initial Sample Range      // This is the range within the leaves in
        Appendix 2—figure 6
        i ← random draw from {0,…,length(θ)−1}
        θ′[i] ← θ[i] + (mutation × sign × scale)                          // Mutate
        Run simulation with θ′
        if leaf passes sanity checks then
            θ ← θ′                                                  // Save new parameters
            break
```

Parameters included in the search

Appendix 2—table 1. Leaf developmental model (***Runions et al., 2017***) parameter names and whether they are allowed to vary in the random walk search (split across three columns).

A value of 1 in the Target column means the parameter was targeted in the walk, 0 means it was not. We split the INITSTATE parameter, which is a vector, up into 13 separate parameters I0–12. I6 is kept at 0; all other parameters are allowed to vary but the values of I0–5 are set to be the reverse of I7–I12. This helps promote symmetrical growth and reduce the occurrence of simulation errors and invalid leaves. Parameters were excluded from the search because some were purely graphical parameters, while others did not vary between the leaves presented in ***Runions et al., 2017*** and were therefore treated as not important determinants of shape. 100/122 parameters were targeted during the simulations.

Parameter	Target	Parameter	Target	Parameter	Target
PSPACE1	1	FAIRING3	1	CPDIST	1
PSPACE2	1	CURVATURE3	1	FILLNONAPICALINTERVALS	1
DISPSTEP	1	STRETCH3	1	NCOMP	0
GDT	1	CFLOW3	1	INTERVAL1	1
FINALFRAME	1	NORMAL3	1	INTERVAL2	1
NUMFLOW	1	TIP_GROWTH3	1	INTERVAL3	1
NSAMP	1	CPDIST3	1	INTERVAL4	1
I_SAMPDIST	1	METRIC3	1	NEWAXISINTS	1
I0	1	EXTENDABLE3	1	NEWAXISINTE	1
I1	1	EXTENDABLE_CONTEXT3	1	FAIRING1	1
I2	1	PATTERNABLE3	1	CURVATURE1	1
I3	1	COMPETENCE3	1	STRETCH1	1
I4	1	COMPETENCET3	1	CFLOW1	1
I5	1	FAIRING4	1	NORMAL1	1
I6	0	CURVATURE4	1	TIP_GROWTH1	1
I7	1	STRETCH4	1	CPDIST1	1

Appendix 2—table 1 Continued on next page

Appendix 2—table 1 Continued

Parameter	Target	Parameter	Target	Parameter	Target
I8	1	CFLOW4	1	METRIC1	1
I9	1	NORMAL4	1	EXTENDABLE1	1
I10	1	TIP_GROWTH4	1	EXTENDABLE_CONTEXT1	1
I11	1	CPDIST4	1	PATTERNABLE1	1
I12	1	METRIC4	1	COMPETENCE1	1
PRIMSCALEX	1	EXTENDABLE4	1	COMPETENCET1	1
PRIMSCALEY	1	EXTENDABLE_CONTEXT4	1	FAIRING2	1
LASSYMETRY	1	PATTERNABLE4	1	CURVATURE2	1
RASSYMETRY	1	COMPETENCE4	1	STRETCH2	1
DIVTHRESH	1	COMPETENCET4	1	CFLOW2	1
MAXANGLE	1	AXISANGLE	1	NORMAL2	1
TIP_GROWTH2	1	CPDIST2	1	METRIC2	1
EXTENDABLE2	1	EXTENDABLE_CONTEXT2	1	PATTERNABLE2	1
COMPETENCE2	1	COMPETENCET2	1	VG_START_X	0
VG_END_X	1	CP_AD_TIP_GROWTH	1	CP_ADTG_FALLOFF	1
AX_AD_AXIS_GROWTH	0	AX_ADAG_FALLOFF	0	APEX_TIP_GROWTH	1
ASYMMETRIC_FAIRING	1	ASYMM_PRE	0	ASYMM_POST	0
SHARP_LEAF_TIP	1	INTERNAL_FLOW	1	PETIOLE_COMPOUND	0
PETIOLE_EXTEND	0	QUADD_ERR_THRESH	0	COMPWIDTH	0
BB_WIDTH_MULT	0	MARGIN_WIDTH	1	SCALE_WIDTH_BY_BB	0
SUPRESSED_COMP	0	PM_POW	0	PM_WIDTH	0
PM_INC	0	PM_SAMP	0	DEFINE_TERMINAL_LEAFLET_BASE	0
BOUNDARY_MORPHOGEN	0	TG_START_X	0	TG_END_X	1
FG_START_X	0	FG_END_X	1	VG_GRATE	1
GLOBAL_RESISTANCE	1	UNIFORM_GROWTH	1		

Agreement between manual and automatic leaf shape classification

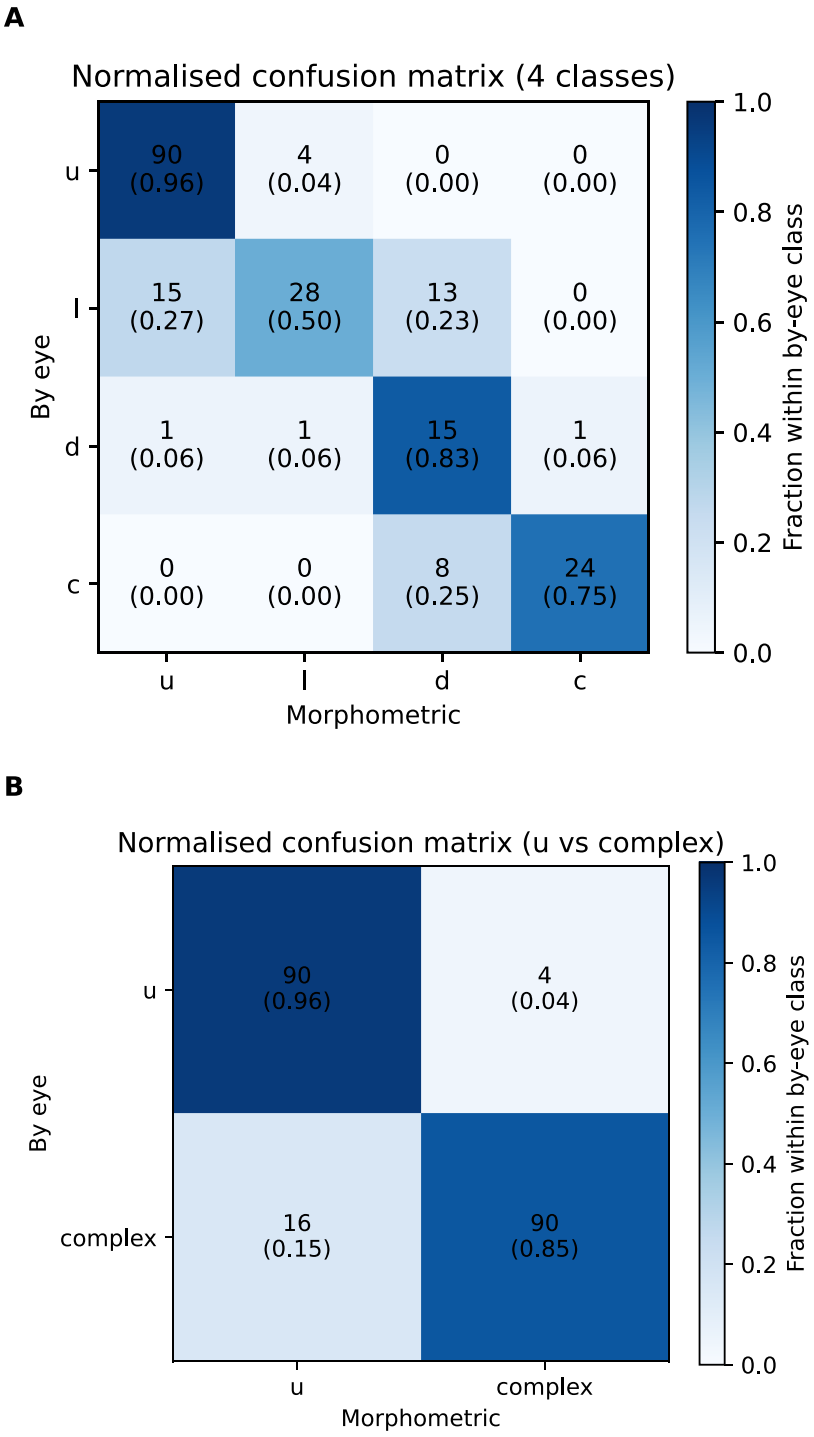

Appendix 2—figure 7. Confusion matrices comparing by-eye and automatic morphometric classification at two resolutions for a sample of 200 simulation leaf images. (**A**) Four-class confusion matrix (u=unlobed, l=lobed, d=dissected, c=compound). (**B**) Binary confusion matrix after collapsing to u and complex, where complex = l ∪ d ∪ c. In both panels, cell colour shows the proportion within each by-eye class, overlaid numbers show raw counts. This comparison is also discussed in Methods: *Shape classification*.

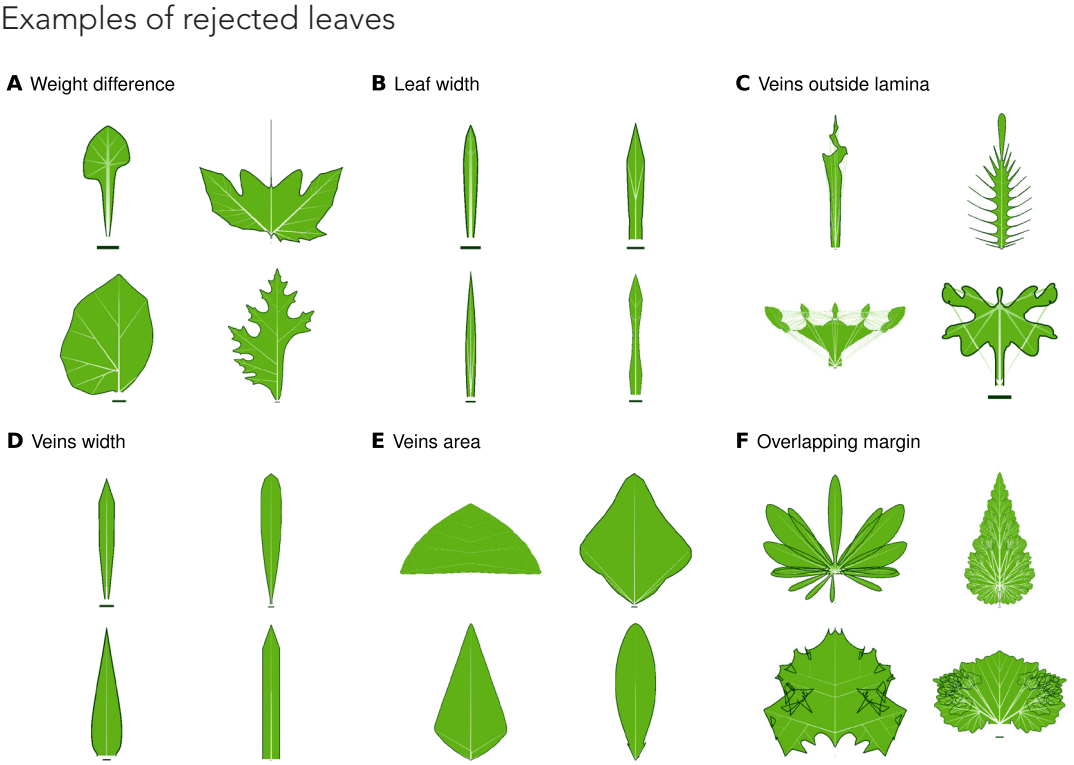

Appendix 2—figure 8. Examples of rejected leaves with the condition (***Table 1***) that each failed to satisfy. (**A-F**) Each leaf shown here passed all conditions except the one stated; however, in general many leaves that are rejected fail multiple conditions.

Appendix 3

Extended phylogenetic methods

Phylogenetic rate inference

We use the MultiState method from BayesTraits V4 to infer transition rates from phylogenetic data. MultiState fits a continuous-time Markov chain (CTMC) to a discrete character distributed across the tips of a phylogeny. The tree topology and character states at the tips are fixed, with only the CTMC parameters defined by the matrix $\boldsymbol{Q}$ being estimated.

The optimal $\boldsymbol{Q}$ is found by maximising the likelihood $\boldsymbol{L}$ of the observed tip data $\boldsymbol{D}$ given the phylogenetic tree $\boldsymbol{T}$ (topology and branch lengths) and the value of $\boldsymbol{Q}$ (***Pagel, 1994***). Let $T = (V, E)$ denote the tree, with leaf nodes $V_{\text{tip}} \subset V$ which have observed states D_v for $v \in V_{\text{tip}}$, and internal nodes $V_{\text{int}} = V \setminus V_{\text{tip}}$ (including the root) which have unobserved states. Under the assumptions of the CTMC, the probability of a single branch $(u, v) \in E$ with parent state x_u, child state x_v and branch length t_{uv} is

$$p(x_u, x_v, t_{uv}) = \left[\exp(\boldsymbol{Q}t_{uv})\right]_{x_u x_v} \tag{3.1}$$

The likelihood is then the product of the probabilities for all branches in the tree summed over all possible assignments of character states at internal nodes (***Pagel, 1994***).

$$L(D|\boldsymbol{Q}, T) = \sum_{\{x_v\}_{v \in V_{\text{int}}}} \prod_{(u,v)\in E} p(x_u, x_v, t_{uv}). \tag{3.2}$$

The pruning algorithm (***Felsenstein, 1981***) is used to compute this likelihood more efficiently. The likelihood surface for $\boldsymbol{Q}$ is then searched, in the case of MLE, to find the value of $\boldsymbol{Q}$ that gives the maximum likelihood solution via the BOBYQA algorithm (***Meade and Pagel, 2024***). In the case of MCMC, a posterior distribution is sampled using Metropolis-Hastings (***Pagel et al., 2004***). This posterior is given by

$$p(\boldsymbol{Q}|D, T) = \frac{p(D|\boldsymbol{Q}, T)p(\boldsymbol{Q})}{\int_{\boldsymbol{Q}} p(D|\boldsymbol{Q}, T)p(\boldsymbol{Q})d\boldsymbol{Q}} \tag{3.3}$$

where $p(D|\boldsymbol{Q}, T) = L(D|\boldsymbol{Q}, T)$, $p(\boldsymbol{Q})$ is the prior distribution and the denominator integrates over all possible values of $\boldsymbol{Q}$. We use uniform priors between 0 and 0.1 for all trees except ***Geeta et al., 2012*** for which we use a uniform prior between 0 and 100. This is because branch lengths for ***Geeta et al., 2012*** are measured in substitutions per site rather than millions of years.

All non-diagonal elements of $\boldsymbol{Q}$ are permitted to vary freely during the fitting process. Diagonal elements are set to the negative sum of other elements in the same row, such that rows sum to zero.

Elements q_{ij} of $\boldsymbol{Q}$ represent the instantaneous rate of transition between state i and j in units of transitions per unit of branch length. To allow comparison between phylogenies with different branch lengths, we normalise the $\boldsymbol{Q}$ matrix for each tree by dividing each transition rate by the mean of the off-diagonal elements of $\boldsymbol{Q}$ (Methods: *Inferring evolutionary rates from phylogeny*).

Phylogenetic tree statistics

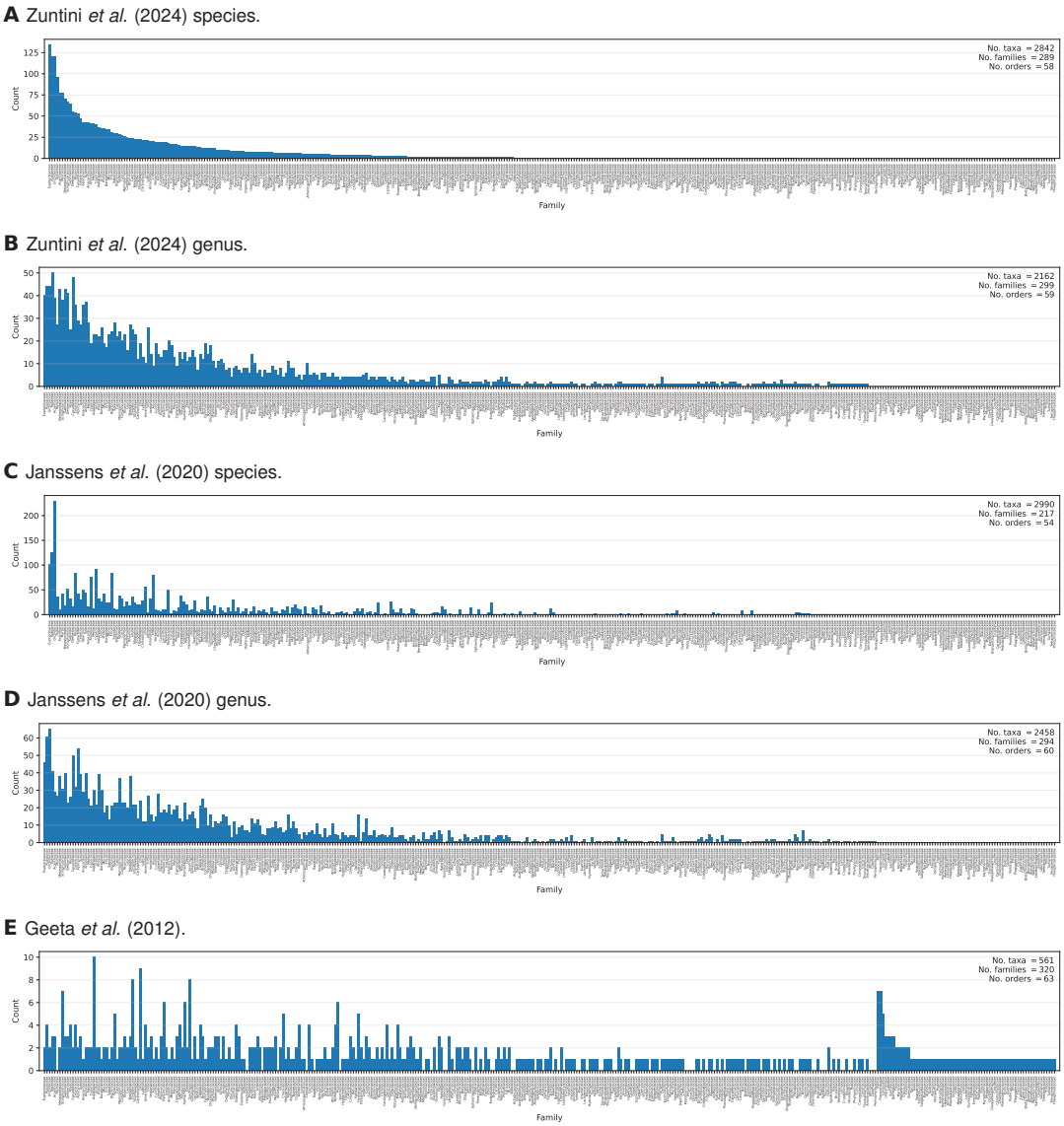

Appendix 3—figure 1. The number of taxa per family across the phylogenetic trees used in our analysis. The distributions are shown for (**A**) the ***Zuntini et al., 2024*** species tree, (**B**) the ***Zuntini et al., 2024*** genus tree, (**C**) the ***Janssens et al., 2020*** species tree, (**D**) the ***Janssens et al., 2020*** genus tree, and (**E**) the ***Geeta et al., 2012*** tree. The distributions are more similar for the ***Zuntini et al., 2024*** genus and ***Janssens et al., 2020*** genus trees than the species trees. This could account for the increased variation in inferred shape transition rates observed between the two species trees relative to the two genus trees (***Appendix 1—figure 1A and B***). Families were assigned to tree tips using data from ***Naturalis Biodiversity Center, 2024***.

Appendix 4

Additional results

PCA occupancy for higher dimensions

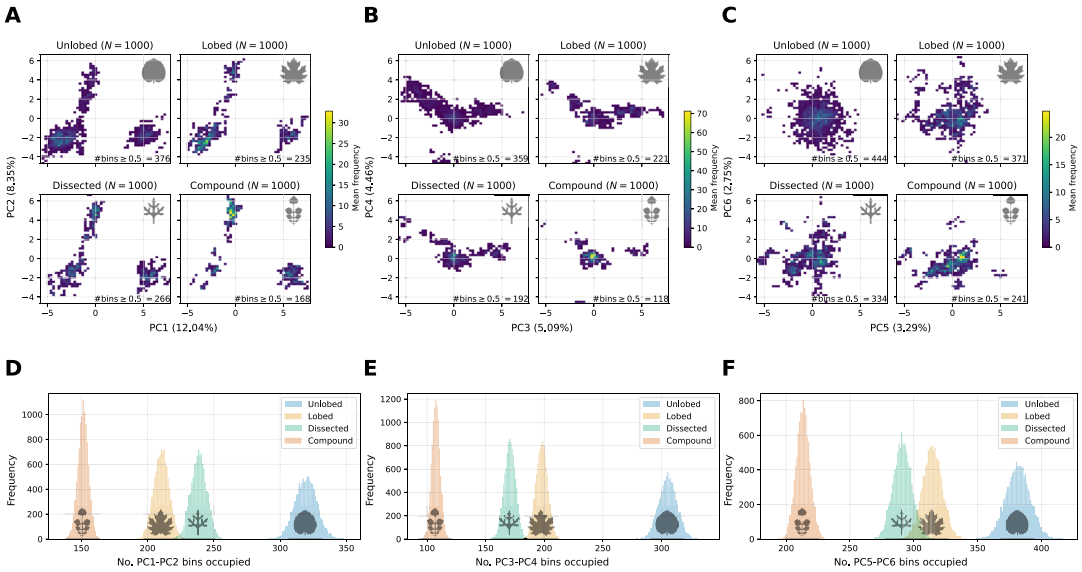

Appendix 4—figure 1. The unlobed category occupies a larger volume within parameter space along principal components 1–6. (**A–C**) 2D histograms of model parameter space for PC1-PC2, PC3-PC4, and PC5-PC6 respectively, showing the distributions of the four leaf shape categories. Note that the regions occupied by more complex shapes continue to overlap substantially with the unlobed domain at higher dimensions. (**D–F**) Distributions of the number of 2D histogram bins occupied by each leaf shape in 10,000 bootstrap samples for PC1-PC2, PC3-PC4, and PC5-PC6, respectively. See ***Figure 4*** for further details of histogram construction and bootstrapping.

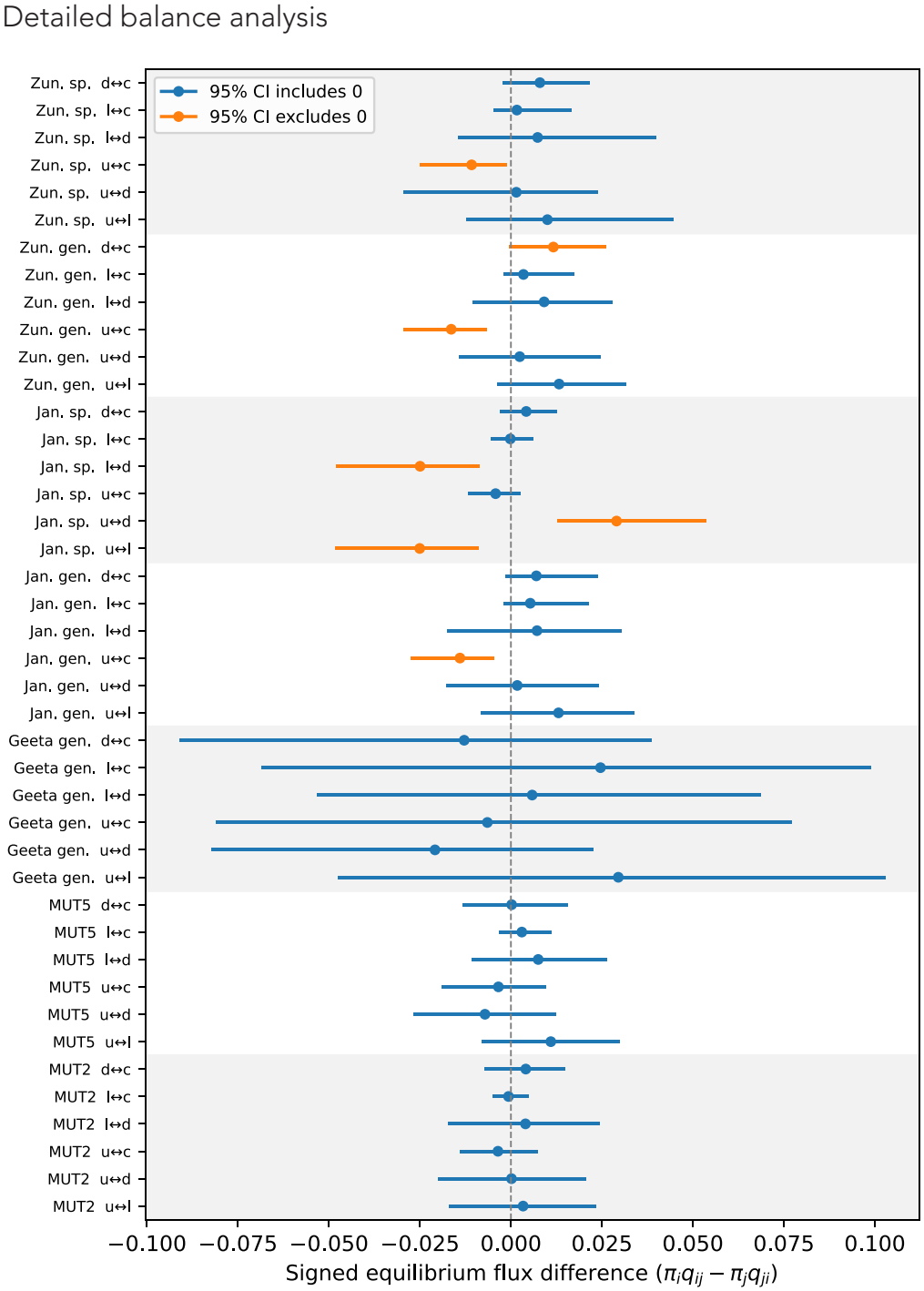

Appendix 4—figure 2. Posterior signed equilibrium flux difference for rate matrices inferred from all simulated and phylogenetic datasets. Each point is the posterior median of $\pi_i q_{ij} - \pi_j q_{ji}$ for a pair of states, where $\boldsymbol{\pi}$ is the stationary distribution over the four states and $\boldsymbol{Q}$ is the posterior rate matrix. The row vector π is defined for each posterior draw of $\boldsymbol{Q}$ by solving $\boldsymbol{\pi Q} = 0$ where $\sum_i \pi_i = 1$. Horizontal bars show 95% credible intervals. Colour shows whether the interval includes zero, indicating consistency with detailed balance, or excludes zero, indicating imbalance. Alternating background bands group state pairs from the same dataset. Simulation transition rates are consistent with detailed balance, as expected given the symmetric mutational schemes (Algorithms 1 and 2.2). Some phylogenetic state pairs are inconsistent with detailed balance, implying potential non-reversibility in the inferred process; however, the affected pairs differ between phylogenetic trees. A positive flux difference means that flux is larger from the first to the second state.

Appendix 5

A short literature review of the adaptive significance of leaf shape

Introduction

As the primary sites of photosynthesis, leaves are critical to plant fitness. They also display extraordinary variation in shape. It is therefore natural to ask to what extent this variation is the product of natural selection. Functional properties of leaves where shape may be relevant include thermoregulation, hydraulic efficiency, biomechanical stability, herbivory defence, light interception and nutrient cycling. Yet, despite an extensive and sophisticated literature, the extent to which leaf shape determines fitness, and hence reflects adaptation, remains the subject of considerable debate. In particular, a recurring difficulty in this literature is distinguishing evidence that morphology affects leaf function from evidence that the resulting functional differences affect fitness, and ultimately from evidence that selection on those differences explains evolutionary patterns of leaf shape.

In this short overview we briefly survey the literature on the role of adaptation in shaping three different classes of shape variables. The first is leaf size, which can vary enormously, from less than $1\,\mathrm{mm}^2$ to over $1\,\mathrm{m}^2$, and correlates quite strongly with climate: it was noted more than a century ago that leaves tend to be large in hot, sunny and wet climates, and small in hot, sunny and arid climates. The second class is marginal leaf teeth, which are small oscillatory patterns or serrations on the margin of leaves. The presence and number of teeth are thought to correlate with mean annual temperature, and have historically been used as a proxy to infer paleoclimate trends. The main class we treat here comprises dissection traits, which are captured by our unlobed, lobed, dissected and compound categories. We note that each of these four dissection categories can exhibit large variations in size, and can be toothed or untoothed.

Size

Leaf size is thought to be particularly important for thermoregulation, hydraulic performance, and light capture. In the case of thermoregulation, leaves need to regulate their temperature to maintain efficient photosynthesis and respiration, prevent damage from heat stress and freezing, and balance heat loss against water loss through transpiration (***Berry and Bjorkman, 1980***; ***Givnish, 1987***; ***Wright et al., 2017***; ***Perez and Feeley, 2020***). Heat exchange between a leaf and the surrounding air depends partly on the thickness of the boundary layer of relatively still air at the leaf surface (***Vogel, 1970***). Smaller leaves generally have thinner boundary layers and therefore exchange heat with the surrounding air more rapidly than larger leaves. A recent large-scale study which analysed 7670 species from 682 sites worldwide (***Wright et al., 2017***) argued that the leaf-to-air temperature difference plays a key role in explaining why large leaves predominate in warm, wet environments, whereas small leaves are common in hot, arid environments and at high altitudes. Interestingly, although these authors did separate out simple from compound leaf shapes, both dissection categories showed similar trends with climate variables.

Leaf size may also influence hydraulic performance. For example, ***Scoffoni et al., 2011*** used simulations and comparisons among 10 species with different drought tolerance to show that smaller leaves with greater major-vein density showed reduced hydraulic vulnerability and greater tolerance to vein embolism. Thus, variation in size may influence both the thermal and hydraulic conditions under which leaves can function. See also ***Sack and Scoffoni, 2013***.

Size is also associated with trade-offs in light capture and resource allocation. Increasing leaf area can increase total photosynthetic surface (***Watson, 1958***), but leaf mass increases with area while proportional gains in area diminish, implying increasing construction costs for larger leaves (***Niklas et al., 2007***). Leaf size additionally interacts with canopy architecture. Smaller leaves may be associated with shorter petioles and greater crowding around stems, potentially increasing self-shading (***Falster and Westoby, 2003***). The leaf economic spectrum further demonstrates that investment in leaf structure is associated with major differences in leaf lifespan and photosynthetic return (***Wright et al., 2004***).

In conclusion, leaf size can have substantial functional consequences and is likely shaped by trade-offs between heat exchange, hydraulic efficiency, construction costs, and light capture. The evidence linking leaf size to ecologically important functions and environmental gradients is arguably stronger than the corresponding evidence for many aspects of leaf shape. Many of the functions affected by

leaf size can also be modified by other aspects of leaf shape. This makes disentangling adaptive from non-adaptive variation more complex.

Teeth

Marginal teeth are shallow projections or serrations separated by sinuses, incised less than 25% of the distance to the midvein (***Ellis et al., 2009***). They are a much less pronounced feature than our dissection categories. Unlobed, lobed, dissected leaves, as well as the leaflets of compound leaves, can be either toothed or untoothed. Indeed, a close look at the first two unlobed leaves in ***Appendix 2—figure 6*** reveals a toothed pattern in one and an untoothed pattern in the other, illustrating that the Runions model (***Runions et al., 2017***) can reproduce this feature on top of the dissection traits.

The presence or absence of leaf teeth has been of particular interest for over a century, due to an observed negative correlation with mean annual temperature (MAT), in particular for woody dicot species (***Bailey and Sinnott, 1916***). The association between climate and leaf tooth presence has been measured repeatedly (***Bailey and Sinnott, 1916***; ***Royer et al., 2005***; ***Peppe et al., 2011***), including by a study across 3549 species and 6 continents (***Royer et al., 2012***). The apparent simplicity and strength of this relationship led to its widespread use to estimate paleoclimate MAT. However, as independent methods for reconstructing past temperatures such as oxygen-isotope measurements and phytoplankton distributions were refined and recalibrated, discrepancies began to emerge between estimates of MAT based on fossil leaf margins and those obtained from these independent paleoclimate proxies. This motivated work to better understand and refine the relationship (***Burnham and Tonkovich, 2011***). Multivariate approaches, particularly Climate-Leaf Analysis Multivariate Program (CLAMP) (***Wolfe, 1993***) or digital leaf physiognomy (***Peppe et al., 2011***), were subsequently developed and refined to incorporate additional aspects of leaf morphology (***Wolfe, 1993***; ***Peppe et al., 2011***). New features, including the shape factor ($4\pi \times \text{blade area/perimeter}^2$), a measure of roundness, were found to correlate with MAT, albeit with a modest amount of variance explained ($r^2 = 0.22, P < 0.001$) (***Peppe et al., 2011***).

However, there are several complicating factors. An important study of 569 species-site pairs that explicitly took phylogenetic models into account demonstrated that ancestry of plant species also plays a significant role in all 21 leaf traits measured, including the abundance of teeth (***Little et al., 2010***). Accounting for shared ancestry decreased the slope of the regression between the presence of teeth and mean annual temperature by an order of magnitude (in log space) to almost a flat line with wider confidence intervals. This suggests that the geographical correlation contains a substantial phylogenetic component, although it does not by itself distinguish whether this arises from phylogenetic constraint, climatic sorting of lineages, or repeated adaptive convergent evolution of toothed or untoothed margins. Subsequent studies suggest that an association between temperature and tooth presence remains after accounting for phylogeny, potentially mediated by venation architecture (***Zohner et al., 2019***), although the picture remains complex (***Li et al., 2016***), and clear counterexamples to the MAT correlation with teeth can also be found in certain species (***Burnham and Tonkovich, 2011***; ***Frye et al., 2020***).

Interestingly, ***Little et al., 2010*** also found that relationships between MAT and more gross shape variables such as shape factor changed little after phylogenetic correction, making these associations more consistent with repeated environmental responses across lineages. However, these correlations are not that strong in the first place. Moreover, the shape factor captures roundness rather than the specific distinctions among unlobed, lobed, dissected, and compound leaves we consider in this study. Overall, an emerging consensus in the field is that evolutionary history and climatic selection jointly contribute to the observed relationship rather than that the relationship is simply a phylogenetic artefact. Modern work on paleoenvironmental reconstruction combines different leaf shape traits with phylogenetic, biogeographic and other analyses rather than relying on the fraction of leaves with teeth alone.

Despite the complications above, many functional hypotheses have been proposed to explain the climate association. Firstly, enhanced early-season photosynthesis at leaf teeth could be particularly advantageous in climates with short growing seasons (***Royer and Wilf, 2006***). Secondly, the 'support-supply' hypothesis posits that cooler climates with short growing seasons favour thinner leaves with stronger veins that penetrate to the margin for which the optimal shape of the surrounding tissue is

wedge-like (**Givnish and Kriebel, 2017**). Thirdly, the 'bud-packing' hypothesis postulates that cold climates favour dense packing of leaf primordia in buds which results in more teeth due to physical forces from folding (**Edwards et al., 2016**). However, the evidence for these is mixed. Although **Royer and Wilf, 2006** show enhanced photosynthesis and transpiration in toothed margins early in the growing season, the extent to which this increases fitness is unclear. Moreover, **Zohner et al., 2019** found that leaf thickness does not predict venation and teeth, contradicting the support-supply hypothesis. They also found that primordium number in buds does not predict margin state, contradicting the bud-packing hypothesis.

In summary, several explanations for the correlation between leaf teeth and MAT remain viable. Teeth may be direct targets of selection because of some functional property they confer, but the relationship could also arise from a more complex combination of adaptive effects, including effects that partly cancel one another or from relatively weak selection. Alternatively, the association between leaf teeth and climate may arise indirectly through selection on other aspects of leaf function. Thus, even for leaf toothiness, where the geographical association with climate is unusually strong and well replicated, identifying the selective mechanism responsible for that association remains difficult. This provides a useful point of comparison for the more pronounced dissection traits considered below, for which geographical correlations are generally less well established.

Dissection and compoundness

In this section we look in more detail at the literature linking leaf dissection traits, measured in our case through the lobed, unlobed, dissected and compound leaf shapes, to a series of different functions of leaves.

Thermoregulation

Thermoregulation is frequently proposed as an important driver of leaf-shape evolution (**Nicotra et al., 2011**). In particular, complex leaves have been hypothesised to behave aerodynamically like many small leaves, resulting in faster heat transfer to the environment (**Leigh et al., 2017**). Laboratory studies using artificial leaves have suggested that leaf heat exchange with the environment is strongly influenced by shape (**Vogel, 1970**). For example, **Vogel, 1970** found that lobed copper plates were more effective heat dissipators than circles. However, this approach ignores other important traits of real leaves (e.g. water content, absorptance) that have large effects on the actual operating temperatures of leaves in natural environments (**Nicotra et al., 2011**).

A more recent study by **Leigh et al., 2017** measured multiple temperature variables in field conditions for 68 Proteaceae species, finding that effective leaf width was a strong predictor of leaf thermal dynamics, whereas leaf margin complexity had no or weak effects. Thus, although dissection can affect convective heat transfer under controlled conditions, its contribution to leaf temperature in vivo may be small relative to other morphological and physiological traits.

Ivyleaf morning glory (*Ipomoea hederacea*) provides an unusually well-studied test case. An investigation of lobed and unlobed genotypes of *Ipomoea hederacea* (**Singhal et al., 2025**) revealed that while both shapes maintain similar temperatures, unlobed phenotypes had significantly increased stomatal conductance in warmer, sunnier conditions. This suggests that unlobed leaves may rely more on latent cooling via transpiration for temperature regulation compared to lobed leaves. The fact that lobed leaves maintain the same temperature without increased stomatal conductance is consistent with a different cooling strategy, perhaps enhanced convective cooling facilitated by the lobed shape to conserve water. This highlights how thermoregulation depends on a range of traits and even if leaf shape is one of them, suboptimal leaf shapes can arise due to trade-offs with these other traits.

Ipomoea hederacea also provides an instructive example of the difficulty of inferring selection from geographical patterns. The species has a clear latitudinal cline in North America, from lobed genotypes in the north to heart-shaped unlobed genotypes in the south, that is known to be determined by a single locus (**Campitelli and Stinchcombe, 2013a**). **Campitelli and Stinchcombe, 2013a** showed that the leaf shape locus displays clinal variation and neutral loci do not, consistent with the leaf shape cline being caused by selection on leaf shape. However, it is possible that selection is acting instead on a different locus in linkage disequilibrium with the leaf shape locus. They suggest that the agent of selection could be temperature. However, contrary to previous studies that

predict that lobes are favoured in hot environments, the lobed genotypes are found more frequently in the colder north end of the cline. To identify the selective agent for this cline, ***Campitelli and Stinchcombe, 2013b*** planted 1680 lobed-unlobed F3 hybrids with varying leaf shape in the north and measured their fitness as well as other selective agents including temperature and herbivory. They found that none of the potential selective agents affected the different leaf shape genotypes differently. This could be because the true selective agent was not among those investigated, or that the cline is not due to selection on leaf shape but is perhaps instead due to selection on another trait in linkage disequilibrium. This study highlights the difficulty in establishing selection as a cause, despite correlations between leaf shape and environmental variables.

Hydraulic efficiency

Leaf shape has also been proposed to influence hydraulic efficiency. Photosynthetic capacity is directly impacted by the efficiency of water transport through leaves, which alone accounts for $\geq 30\%$ of the total resistance to water flow through plants (***Sack and Frole, 2006***). Leaf structure, particularly venation architecture, strongly affects the strength of this resistance.

Sisó et al., 2001 found that in seven species of oak (*Quercus*), leaves with increased lobation had lower hydraulic resistance. It is thought that this is caused by a lower ratio of mesophyll tissue to vasculature in lobed leaves. This is consistent with the hypothesis that deeply lobed leaves may be a way of improving water balance in arid environments.

On the other hand, ***Sack and Frole, 2006*** investigated the relationship between leaf structure and hydraulic resistance in 10 coexisting tropical rain forest tree species in Panama. They found that while resistance was negatively associated with vein density, there was no significant association with shape. Moreover, ***Scoffoni et al., 2011*** found, through simulations and comparisons among 10 diverse species with highly varying drought tolerance, that smaller leaves with higher major vein density had reduced hydraulic vulnerability and higher tolerance to vein embolism (the blocking of veins by air bubbles).

Therefore, while shape may have some effect on hydraulic efficiency, properties of the vasculature, such as vein density, may more directly determine hydraulic function.

Biomechanical stability

Leaves are constantly subjected to various mechanical stresses from their environment, including static loads such as their own weight, accumulated snow or ice, and dynamic loads primarily from wind and rain. In order to maintain optimal fitness-critical functions such as photosynthesis, they need to withstand these stresses with minimal damage and maintain optimal positioning for light interception. Much of the biomechanical literature concerns dimensions or petiole properties rather than dissection per se. However, it is possible that leaf shape affects the ability to withstand mechanical stress and therefore has been optimised by natural selection for mechanical robustness, particularly in high-stress environments (e.g. windy environments).

Tadrist and Darbois-Texier, 2016 found that they could predict scaling relationships among palm leaf length, width, thickness and petiole diameter with a mathematical model that maximises surface area under gravitational self-support constraints. This suggests that for this particular group of large-leaved plants, leaf dimensions may be constrained by optimisation for self-support. It is not clear how important other shape features, such as margin complexity, are for self-support.

Moreover, ***Louf et al., 2018*** predicted a relationship between blade aspect ratio and the relative bending and twisting rigidity of petioles, which was broadly consistent with measurements from four broad-leaved species. This is consistent with adaptive trade-offs between leaf shape and petiole mechanical properties as a result of mechanical stress from wind.

Niklas, 1996 found that leaves from wind-exposed and protected sugar maple trees (*Acer saccharum*) differed significantly in some aspects of shape. Leaves from wind-exposed trees had smaller surface areas and shorter and narrower petioles that were less rigid than petioles from leaves on protected trees. These differences are thought to be due to adaptive phenotypic plasticity in response to chronic mechanical perturbation by wind. The shorter, more flexible petioles allow for easier twisting and bending in response to the wind, reducing drag forces and the chance of mechanical tissue damage (***Niklas, 1999***).

Different leaf shapes experience different levels of drag, relative to their surface area, in response to wind. Through wind-tunnel experiments, ***Vogel, 1989*** found that pinnately compound leaves had lower drag than clusters of simple leaves by reconfiguring into a streamlined cylinder shape with alternately layered leaflets. This demonstrates a physical effect of leaf shape on drag and reconfiguration in wind, although whether this translates into differences in fitness remains to be established.

Herbivory defence

Leaf herbivory is costly to plant fitness by reducing photosynthetic capacity. Leaves have evolved many features that deter herbivores such as chemical toxicity and physical barriers such as the waxy cuticle, thorns and trichomes. The role of leaf shape is less obvious; nevertheless, there is some evidence that it can impact herbivory.

For example, ***Higuchi and Kawakita, 2019*** showed that the leaf-rolling weevil *Apoderus praecellens* could be deterred from cutting the leaves of its host genus *Isodon* by replacing leaves from an unlobed species (*I. trichocarpus*) typical of the genus with lobed leaves from a closely related species (*I. umbrosus*). They controlled for potential confounding differences between the plant species by cutting lobes into *I. trichocarpus* leaves to resemble *I. umbrosus*, and still found a preference for the unlobed *I. trichocarpus* leaves among the female weevils.

Moreover, there is observational (***Rausher, 1978***) and direct experimental (***Dell'Aglio et al., 2016***) evidence that ovipositing butterflies use vision to recognise plant hosts by leaf shape and can have a preference for some shapes over others. This shows that butterflies have the potential to exert selection on leaf shape in host species.

On the other hand, ***Campitelli et al., 2008*** investigated how alternative leaf morphs of the *Ipomoea hederacea* affect the performance (e.g. insect biomass, leaf area consumed, digestive efficiency) of three different generalist insect herbivores. They found that the effect of shape on performance was highly variable between insect species, plant developmental stage and growth conditions. Therefore, while some insect herbivores may be able to consume certain leaf shapes more easily, it seems there is no consistent trend and other plant traits may play a more significant role.

Light interception and optimisation

Leaves function as the primary organs for light harvesting in vascular plants and are therefore of utmost importance to photosynthetic capacity. While the effects of several non-shape traits on photosynthetic capacity are well understood, the effect of shape per se is more uncertain (***Nicotra et al., 2011***).

Simulations of maize (*Zea mays*) have found that variation in leaf shape can alter light interception by up to 7% (***Otto et al., 2025***). *Z. mays* leaves do not vary as substantially in shape as those of other lineages, suggesting that the effect on light interception may be greater for other plants with more shape variation.

Further simulations in oil palm found that parameters related to leaf area had the largest effect on light interception and carbon assimilation, and the effect of other shape parameters was less important (***Perez et al., 2018***).

Several studies on poplars have shown that some aspects of leaf shape can evolve to reduce self-shading within canopies. Aspen (*Populus tremuloides*) has evolved a flattened, non-rigid petiole oriented perpendicular to the leaf blade, resulting in enhanced leaf flutter even in light winds (***Roden, 2003***). By directly measuring light intensity at different points within the canopy of two poplar species, ***Roden and Pearcy, 1993a*** showed that leaf flutter increased light penetration into the lower canopy, creating a more spatially even understory light environment. This can enhance whole canopy carbon gain, as understory poplar leaves are very efficient at utilising rapidly fluctuating light environments for photosynthesis (***Roden and Pearcy, 1993b***). Furthermore, evidence from simulations suggests that fluttering leaves at the top of the canopy have more uniform light interception than static leaves and therefore also potentially enhanced carbon gain (***Roden, 2003***). This highlights how leaf shape can indirectly alter light interception by altering the mechanical response to wind. It is not clear how the shape of parts of the leaf besides the petiole could affect flutter.

Donoghue et al., 2022 identified a link between leaf morphology and light levels in geographically isolated populations of *Viburnum* in Mexican and South American cloud forests. These populations showed convergent evolution of different leaf ecomorphs, consistent with repeated adaptive evolution into the same niches across these isolated locations. However, the authors did not rule out neutral evolution as a potential cause. By measuring environmental variables in these isolated populations, they identified a positive correlation between large leaves, lower light levels and higher wetness. This is consistent with the hypothesis that larger leaves are an adaptation to lower light environments, but does not prove any differences in fitness associated with leaf shape. Moreover, the main correlation they found was related to size rather than shape.

Nutrient cycling

Deciduous trees shed their leaves annually, avoiding the cost of maintaining foliage under the stress of winter. However, this results in these trees losing 40% of their assimilated carbon and substantial amounts of nitrogen, phosphorus, potassium and other nutrients (***Biviano and Jensen, 2025***). Given the potential nutritional value of these leaves, it is possible that there is a fitness benefit to trees that deposit their leaves nearby, such that their nutrients can be recycled and local soil conditions are improved. ***Biviano and Jensen, 2025*** investigated the hypothesis that symmetric and unlobed leaves may have evolved as a strategy to increase leaf settling speed such that fallen leaves land closer to the tree of origin, facilitating nutrient retention. Through experiments with paper leaves, they found that highly symmetric shapes settled the fastest, with increasing lobedness decreasing settling speed. Asymmetric shapes settled substantially more slowly and were largely insensitive to changes in lobedness. This is consistent with the notion that leaf shape may also be under selection to facilitate nutrient recycling by maximising settling speed.

Conclusion

While the evidence for adaptation is much weaker for these dissection categories than it is for leaf size or even teeth, there remains substantial evidence that leaf dissection and compoundness can influence thermoregulation, hydraulics, mechanical behaviour, herbivore interactions and light interception. However, most studies establish functional effects rather than fitness consequences, and many are restricted to particular species or lineages. Moreover, in several cases leaf size, venation or petiole architecture appear to have stronger functional effects than dissection itself. Dissection may therefore be adaptive in particular ecological contexts, and different selective pressures may favour similar shapes in different contexts, but there is currently limited evidence for a general selective explanation for its broad evolutionary distribution. Absence of evidence is not necessarily evidence of absence. So, while there may still be an adaptive explanation, or several explanations, for the higher evolutionary transition rates towards unlobed shapes than complex shapes—lobed, dissected and compound—the current literature does not offer a clear answer to what this might be.